



Climate-controlled sensitivity of lake sediments to record earthquake-related mass wasting in tropical Lake Towuti during the past 40 kyr

Nicolas Tournier^{a, *}, Stefano C. Fabbri^{a, b}, Flavio S. Anselmetti^a, Sri Yudawati Cahyarini^c, Satria Bijaksana^d, Nigel Watrus^e, James M. Russell^f, Hendrik Vogel^a

^a Institute of Geological Sciences & Oeschger Centre of Climate Change Research, University of Bern, Baltzerstr. 1+3, 3012, Bern, Switzerland

^b Edytem, Université Savoie Mont-Blanc, CNRS, 5, bd de la Mer Caspienne, Le Bourget-du-Lac, France

^c Research Centre for Climate and Atmosphere, National Research and Innovation Agency (BRIN), Indonesia

^d Faculty of Mining and Petroleum Engineering, Institut Teknologi Bandung, 15 Bandung, 40132, Indonesia

^e Large Lakes Observatory & Dept. of Earth and Environmental Sciences, University of Minnesota Duluth, Duluth, MN, 55812, USA

^f Department of Earth, Environmental, And Planetary Sciences, Brown University, Box 1846, Providence, RI, 02912, USA

ARTICLE INFO

Article history:

Received 29 August 2022

Received in revised form

14 February 2023

Accepted 19 February 2023

Available online xxx

Handling Editor: Giovanni Zanchetta

Keywords:

Paleoseismology

Paleoclimate

Lake-level change

Seismic stratigraphy

Late Pleistocene

Sulawesi/Indonesia

ABSTRACT

Located at the triple junction of the Pacific, Eurasian and Sunda plates, the Island of Sulawesi in Indonesia is one of the most tectonically active places on Earth. This is highlighted by the recurrence of devastating earthquakes such as the 2018 Mw 7.5 earthquake that damaged the city of Palu and caused several thousand fatalities in central Sulawesi. The majority of large-magnitude earthquakes on Sulawesi are related to stress release along major strike-slip faults such as the Palu-Koro Fault and its southern extensions, the Matano and Lawanopo Faults. To date, information on the frequency and magnitude of past major events on these faults is limited to instrumental records and historical sources restricted to the last century, whereas information from natural archives is completely lacking. Lake-sediment records can fill this gap, but a detailed assessment of the various factors that influence the sensitivity of sediment successions to past earthquakes is required to evaluate their suitability. Lake Towuti, situated in Eastern Sulawesi, is known for its paleoclimate record and also promises to be a key site to generate a paleoseismology record for Sulawesi. The lake lies close to the highly active Matano and Lawanopo strike-slip faults and thereby is an ideal archive for past earthquakes that have occurred in the surrounding area. Here we combine high-resolution chirp seismic data with lithostratigraphic and petrophysical data of sediment piston cores to assess the recurrence of seismically generated mass-transport and turbidite deposits. Three major seismic-stratigraphic units are distinguished in the upper ~10 m of the sediment succession and linked to differences in the frequency of mass-wasting during the past 60 kyrs. The evidence of a more turbidite-prone period between 12 and 40 ka is roughly coincident with a dry phase and associated lake-level lowstand during the last glacial period at Lake Towuti. Hence, we suggest that climate strongly influences the sensitivity of slopes to fail during seismic shaking in this tropical setting as a consequence of lowstand-forced sediment redeposition from the shelves onto the slopes and into the basins. As climate significantly impacts the sensitivity of the lacustrine sediments to record earthquake-related mass wasting deposits, we suggest that the frequency of mass-transport deposits can additionally be employed as a quantitative indicator for past changes in hydroclimate in these tropical settings.

© 2023 The Authors. Published by Elsevier Ltd. This is an open access article under the CC BY license (<http://creativecommons.org/licenses/by/4.0/>).

1. Introduction

When the crustal deformation rate of a region is low, or when

the release of fault energy through small earthquakes is frequent, there is a necessity to observe major seismic events over long time periods to successfully reveal their recurrence pattern (Lafuente et al., 2014; Moernaut et al., 2014). This relates to the extended recurrence period of strong earthquakes that is often longer than the time covered by both instrumental and historical records (Kremer et al., 2017). To identify periods and regions with more

* Corresponding author.

E-mail address: nicolas.tournier@geo.unibe.ch (N. Tournier).

active seismic activity and to evaluate fault activity and evolution, it is therefore necessary to extend our knowledge of the temporal and spatial distribution of seismic events.

The Island of Sulawesi, in Eastern Indonesia, is located on the 'Ring of Fire' that encircles the entire Pacific Ocean. Consequently, it is subject to frequent and severe earthquakes (Bellier et al., 2001). In 2018, a magnitude 7.5 earthquake in Palu (Bao et al., 2019; Omira et al., 2019; Wu et al., 2021) caused several thousand fatalities and massive material damage. The earthquake-induced damage was further enhanced by an associated tsunami heavily affecting the shorelines along the Gulf of Palu. Seismic events of this magnitude are regarded as exceptional in the region, though, based on the documented and recorded 13 moment magnitude (Mw) 7+ earthquakes since 1924, they occur on average every decade on the Island of Sulawesi. Less powerful earthquakes strike more frequently. About one Mw 6.0 to 6.9 earthquake occurs every year and Mw 5.0 to 5.9 earthquakes occur nine times per year on average (depths <35 km), as documented in the Sulawesi earthquake catalogue (1924–2022) of the International Seismological Center (ISC) (Willemann and Storchak, 2001). The Island of Sulawesi is segmented by three major strike-slip faults (Fig. 1): the Palu-Koro (PKF), the Matano (MF) and the Lawanopo (LF) Faults. These faults cut across the island from NW to SE and define a major transform zone between the eastern and the western parts of the island (Fig. 1A), between the North Sulawesi Trench and the Tolo thrust (Silver et al., 1983). The entire Island of Sulawesi is split into multiple rotating tectonic microblocks, which accommodate the entire collision of the area by crustal rotation rather than by orogenesis. While the south-eastern part of Sulawesi rotates anticlockwise, the north-eastern part rotates clockwise (Socquet et al., 2006). Most of the earthquakes, and particularly the shallow large magnitude ones, typically have their epicenters along the three

crustal faults PKF, MF and LF. Therefore, stress is generally transferred via left-lateral movement along those faults, accompanied by a rotation of various tectonic microblocks (Socquet et al., 2006; Villeneuve et al., 2002), rather than by crustal shortening. Earthquakes are also concentrated along the North Sulawesi subduction zone (Fig. 1).

The oldest earthquakes on Sulawesi recorded by the United States Geological Survey (USGS) and the ISC date back to the early 1900s. To date, only few paleoseismological studies are available to extend the earthquake catalogue beyond instrumental and historical records (Irsyam et al., 2020; Natawidjaja et al., 2020). However, the expansion of our knowledge of the region's seismic event history is vital to improve our understanding of the seismic and tsunamigenic hazard in the region (i.g. Daryono et al., 2021; Watkinson and Hall, 2017; Wils et al., 2021b). Given the severity of the few instrumentally recorded earthquakes and the population increase in city centres and agglomeration areas, better estimates on the earthquake cycle (e.g. recurrence period and pattern) are essential. The September 2018 Mw 7.5 earthquake in Palu has recently generated considerable attention to the hazard potential of the PKF while such awareness is currently absent for other areas of Sulawesi. For example, the south-eastern part of Sulawesi remains poorly studied despite the presence of the similarly active MF and LF. Historical events call for the generation of a paleorecord of similar events, which will allow better estimates of recurrences and magnitudes and, consequently, better adaptation to these natural hazards through mitigation measures (building stability, education, etc.).

Lake Towuti represents the ideal site to generate a long regional paleoseismic record. It has a continuous >1 Myr sedimentary record (Russell et al., 2020b), large surface area-to-depth ratio with gently inclined slopes (Morlock et al., 2019; Vogel et al., 2015)

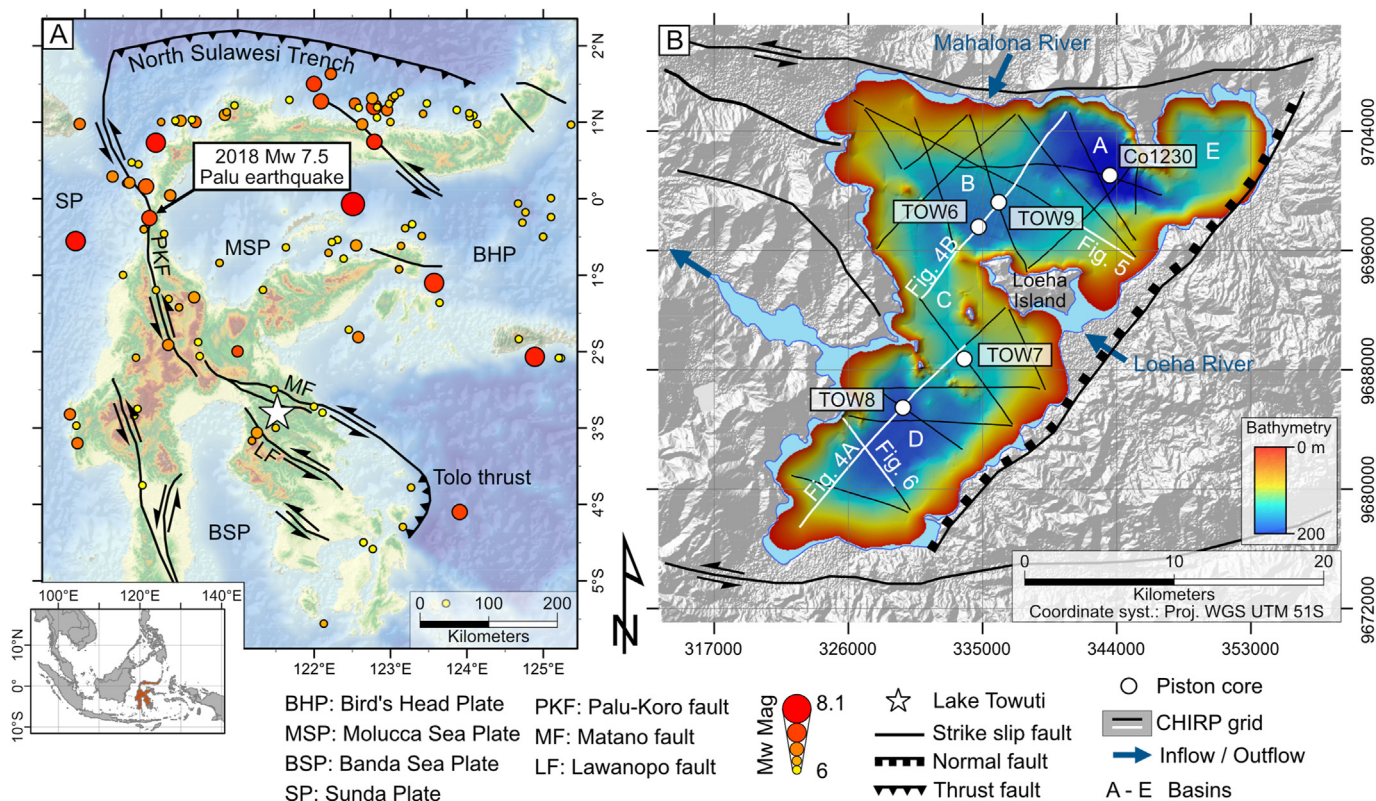


Fig. 1. (A) Seismo-tectonic map of the Island of Sulawesi. Earthquakes from 1924 to 2022 are displayed, with a Mw magnitude ≥ 6 and a depth ≤ 35 km. (B) Bathymetric map of Lake Towuti with the high-resolution CHIRP seismic grid and the location of the piston cores.

necessary for off-fault recording of seismic shaking (e.g. turbidites, mass movements), a large number of available drill and piston core records (Russell et al., 2020b, 2014; Vogel et al., 2015), and a dense grid of seismic reflection data (Russell et al., 2016). Tectonically, the Towuti basin formed by fault movement of the MF (an eastward extension of the PKF) and its conjugated fault structures, making it possible to directly analyse the creation of tectonically-controlled sediment accommodation space on local and regional scales. However, the lake and its catchment also experienced considerable changes in climate, lake level and land cover over its ~1 Myr history (Russell et al., 2020b), making it essential to understand how these environmental processes might interact with tectonic changes to influence the lake's paleoseismic record.

The sedimentary fill of lakes represents a continuous timeline over thousands of years, very sensitive to climatic (Ariztegui et al., 2001; Guyard et al., 2007), seismic (Avşar et al., 2015; Chapron, 1999; Howarth et al., 2021, 2014; Oswald et al., 2021; Schwestermann et al., 2020; Strasser et al., 2013; Talling, 2021) and volcanic (Chassiot et al., 2016; Shinohara et al., 2015) processes. Lakes constitute an essential archive for the study of geological events and processes and are among the very few continental depositional environments that continuously record changes over geological time-scales. Most long-lived lakes form in volcanic (Moernaut et al., 2010; Wils et al., 2021a), impact (Melles et al., 2012; Shanahan et al., 2006) or tectonically active areas involving either extensional (e.g. East African Hutchinson et al., 1992; Russell et al., 2020a), collisional (subduction zones in Chile, Alaska, Japan, Chapron et al., 2006; Inouchi et al., 1996; Kempf et al., 2020; Moernaut et al., 2014; Praet et al., 2017), transtensional regimes (Gastineau et al., 2021; Hage et al., 2017; Hubert-Ferrari et al., 2020) or a combination thereof (e.g. Japan and Indonesia, Shiki et al., 2000; Watkinson and Hall, 2017), creating and sustaining accommodation space over time, and hence making them invaluable paleoseismology archives. Therefore, lakes are ideal sites to provide a better understanding on earthquake recurrence patterns, fault behaviour and seismic hazard assessment.

Several criteria have to be met for a lacustrine setting to serve as an ideal archive of past earthquake events. Most importantly, factors such as sedimentation rate and earthquake intensity are critical (Wilhelm et al., 2016). Generally, low sedimentation rates cause a slow charging of subaqueous slopes with fresh sediments, and therefore the probability to record earthquake-induced subaqueous mass movements may be low, leading to a less sensitive setting (Moernaut, 2020). On the other hand, sites characterized by lower sedimentation rate offer more easily accessible long-term records through sediment coring. Slope inclination is also a significant factor in the susceptibility of lakes to experience sediment failures (Pohl et al., 2020). A steeper slope increases the gravitational stress relative to the strength and stability of the sediments. However, a gentle inclined slope can also generate mass movements and soft sediment deformations (Avşar et al., 2016; Molenaar et al., 2021), especially following an earthquake (Field et al., 1982). During seismic shaking, liquefaction can destabilize the sediments either on land, as documented by the devastating landslide triggered by the 2018 Palu earthquake (Tohari et al., 2021; Watkinson and Hall, 2019), or within water filled basins (Boncio et al., 2020). Several studies indicate an intensity of $\geq VI$ is necessary to trigger mass-transport deposits (MTDs) and the formation of turbidites, and minimum VII1/2 for the development of massive slope failures and megaturbidites (Moernaut et al., 2007; Van Daele et al., 2015; Vanneste et al., 2018). Systematic turbidite-paleoseismological approaches have been successful in several regions that meet these criteria, like in Cascadia (Goldfinger, 2011; Leithold et al., 2019, 2018), New-Zealand (Howarth et al., 2021, 2014),

Mediterranean (Badhani et al., 2020; Ratzov et al., 2015), Southwest Iberian margin (Collico et al., 2020; Gràcia et al., 2010), Alaska (Praet et al., 2020, 2017), European Alps (Chapron et al., 2016; Daxer et al., 2022; Kremer et al., 2015; Schnellmann et al., 2005; Strasser et al., 2020) and Chile (Chapron et al., 2006; Moernaut et al., 2018; Völker et al., 2012; Wils et al., 2020) as well as in other regions (Inouchi et al., 1996; Nayak et al., 2021).

A connection between water-level fluctuations and MTDs has already been proposed for different settings (ten Brink et al., 2016), such as in Patagonia (Anselmetti et al., 2009), East Africa (Moernaut et al., 2010), New Jersey continental margin (McHugh et al., 2002), and the Dead Sea (Waldmann et al., 2009), the latter of which has a tectonic strike-slip fault context similar to that of Lake Towuti (Bartov and Sagy, 2004). For the Dead Sea, a link between climate-controlled lake-level fluctuations (Bartov et al., 2002; Bookman et al., 2006; Goldstein et al., 2020) and the occurrence of submarine mass failures has been documented (Belferman et al., 2018; Closson et al., 2010; Dente et al., 2021; Lu et al., 2021b). Lowstands from 35 ka to 15 ka, may have caused slope erosion and decreased the stability of the emerged areas around the lake (Lu et al., 2021a).

This study forms part of the International Continental Scientific Drilling Program (ICDP) co-funded Towuti Drilling Project (TDP, Russell et al., 2020b; 2016). Previous and ongoing investigations on piston cores from site surveys and cores from scientific drilling document that Lake Towuti is highly sensitive to record past changes in hydroclimate. Evidence from various sedimentological and geochemical indicators suggests the region has experienced substantial drying during the last glacial between ~29 and 16 kyr BP, roughly coincident with marine isotope stage (MIS) 2 and broadly consistent with other reconstructions from the region (De Deckker et al., 2003; Konecky et al., 2016; Krause et al., 2019; Ma et al., 2022; Partin et al., 2007; Reeves et al., 2013; Windler et al., 2020). Drying during the last glacial led to lake-level lowstands with basinward progradation of major deltas (Morlock et al., 2019; Vogel et al., 2015), opening of the local forest vegetation (Hamilton et al., 2019; Russell et al., 2014; Wicaksono et al., 2017), reduced terrestrial runoff (Morlock et al., 2021, 2019; Russell et al., 2014, 2020b) and deep mixing and oxygenation of the water column (Costa et al., 2015; Tamuntuan et al., 2015). These climatically driven environmental and depositional changes are likely to influence the sensitivity of Lake Towuti and, more broadly similar tropical sites, to record past earthquakes. Lake Towuti may therefore represent the ideal site to explore the interplay of climatic and depositional processes on the sensitivity of lacustrine settings to document the impact of past earthquakes.

Here we aim at generating an event stratigraphy based on seismic reflection and sediment-core data from Lake Towuti. The correlation of these analyses permits us to: (1) understand depositional processes occurring within and across the different stratigraphic and seismic units, (2) identify earthquake-related structures and deposits and their temporal relationships, (3) contribute to creating a paleoseismic record for the Malili Lakes region of East-Sulawesi, and (4) explore the effect of (hydro-) climate changes and associated lake-level fluctuations on the sensitivity to record past earthquakes in tropical settings.

2. Regional setting

The Island of Sulawesi (Fig. 1), in eastern Indonesia, comprises four elongated arms with a diverse geology that includes volcanic extrusives underlain by metamorphic rocks to the west, outcropping metamorphic rocks in the central part and ophiolites that are partly covered with sedimentary rocks to the east (Villeneuve et al., 2002). The obduction of the East Sulawesi Ophiolite (ESO) is related

to the interaction of the Eurasia, Indo-Australia and Pacific plates forming a triple junction since the Late Mesozoic to Oligocene (Kadarusman et al., 2004; Villeneuve et al., 2002).

The Malili Lakes are located within Sulawesi's southeast arm forming a drainage basin that is tectonically active and characterized by major strike-slip faults with oblique components (Fig. 2). The three largest lakes of the Malili system (Matano, Mahalona and Towuti) are interconnected while the two other lakes (Lontoa and Masapi) are presently not connected. The formation of this ancient lake system is thought to have taken place 1 to 4 Ma ago (Russell et al., 2020b) following the activation of transform faults in the Early Miocene (Hall and Wilson, 2000), with Lake Matano thought of being the oldest lake (Vaillant et al., 2011). The catchment is predominantly composed of ultramafic bedrock (harzburgite peridotite and lherzolite; Hasberg et al., 2019) with minor associations of more mafic rocks (Costa et al., 2015). These mafic and ultramafic rocks are interspersed with Mesozoic limestones or Tertiary sandstones and shales (Hamilton, 1972). Bedrock in the catchment is

transformed to thick lateritic soils, which supply the lake with substrates high in redox-sensitive metals such as iron, nickel, and chromium (Crowe et al., 2008).

Lake Towuti formed around 1 Ma ago within a transtensional basin created by the predominant strike-slip motion along the MF (Russell et al., 2020b). The lake has a maximum depth of 203 m, lies at 319 m a.s.l. and represents the most downstream lake in the Malili Lake system. Lake Towuti is hydrologically open with a surface area covering 560 km² and a watershed comprising 1145 km² (Morlock et al., 2019). The Mahalona River drains 25% of the Lake Towuti watershed dominated by Quaternary alluvial deposits (Hasberg et al., 2019; Morlock, 2018). To the east of the lake, the Loeha River partly drains metasedimentary rocks and supplies felsic minerals to the lake. To the south, three rivers drain 10% of the watershed composed of ultramafic rocks. The remaining shoreline to the north and west is dominated by steep slopes and dense vegetation, without permanent rivers. Lake Towuti has an average annual temperature of 25.7 °C, with monthly variations lower than

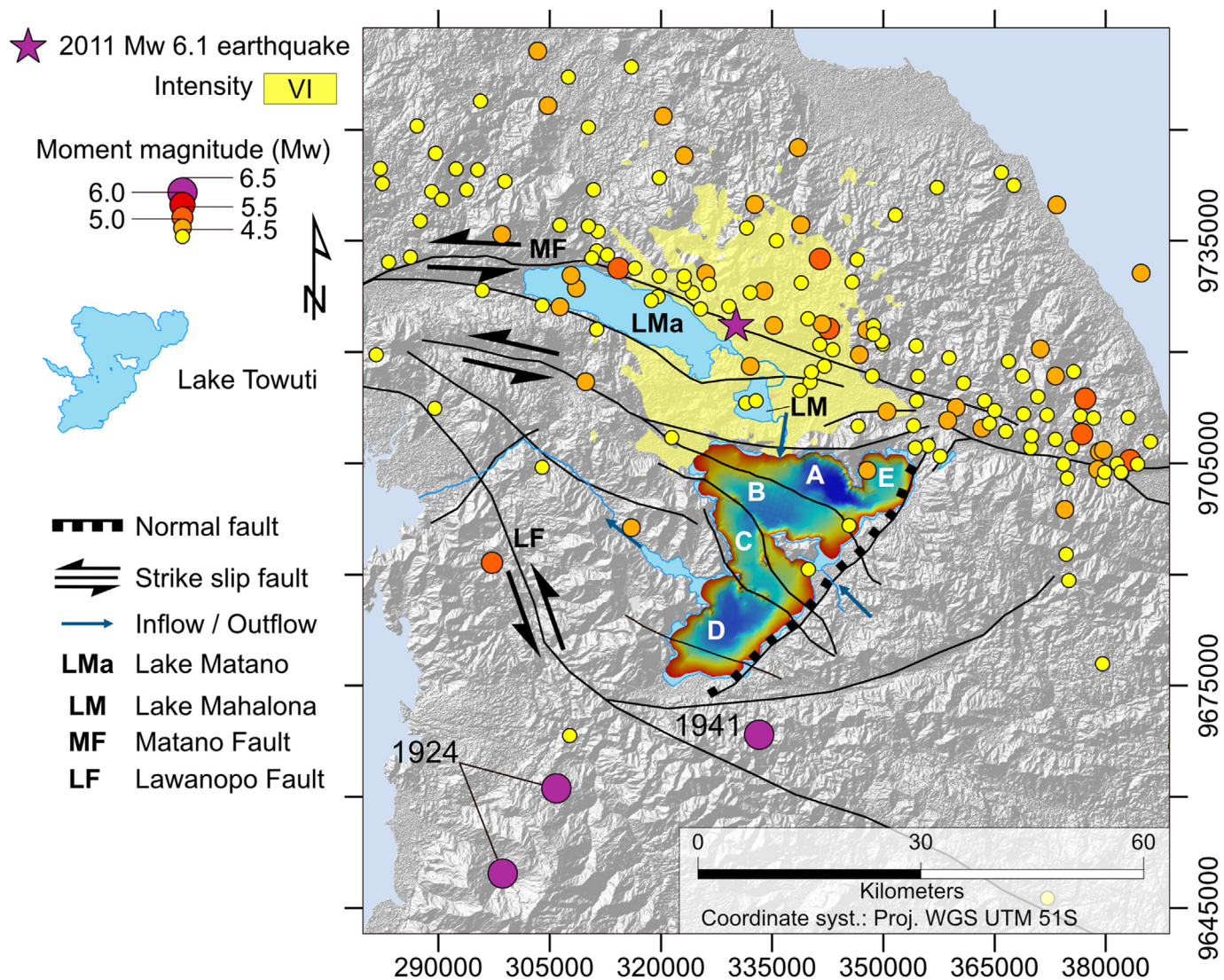


Fig. 2. Map of the Malili system and the Matano and Lawanopo faults (from Watkinson and Hall, 2017) showing historical earthquakes. The earthquake catalogue originates from the International Seismological Center (ISC), with only events of magnitude ≥ 4 , depth ≤ 35 km, between 1924 and 2021 shown (Supplementary Material Table S2). The majority of the seismic events are located along the Matano Fault. The 2011 Mw 6.1 earthquake (purple star) affected the northern shoreline of Lake Towuti with an intensity of VI (Shakemap by USGS Earthquake Hazards Program; <https://earthquake.usgs.gov/earthquakes/eventpage/usp000huj/shakemap/intensity>, modified accessed in Feb. 2022). The labels A-E are the five basins delineated by the faults.

1 °C (Vogel et al., 2015). The maximum precipitation is in April and the minimum in August, for an annual average of 2540 mm. The annual cross-equatorial movement of the Intertropical Convergence Zone (ITCZ) and the Australo-Indonesian Summer Monsoon (AISM) control most of the seasonal rainfall distribution. The lake is also affected by El-Nino events, which can induce a decrease in lake level, such as the 3–5 m decrease during the 1997–1998 event (Tahid et al., 2000).

The three strike-slip faults are highly active, with displacements of ~30–50 mm/year for the PKF (Bellier et al., 2006; Stevens et al., 1999; Watkinson and Hall, 2017). Displacement rates for the MF and LF are not as accurately documented as for the PKF, but the geomorphic features and their conjugated position in relation to the PKF point to a similar rate in the order of tens of mm/year (Costa et al., 2015). These fault structures induce the formation of trans-tensional basins, like Lake Towuti, which are common features in a strike-slip faulting context (Ballance and Reading, 1980). This conjugated strike-slip fault system is responsible for most of the earthquakes in the region. Since the early 20th century, 150 earthquakes with $M_w \geq 4.5$ and depths ≤ 35 km have occurred along the main strand of the MF and LF in the Malili Lakes area (Fig. 2, Willemann and Storchak, 2001). Amongst these events, the 2011 $M_w 6.1$ earthquake, with its epicenter on the MF, damaged the only hospital within a 100 km radius (Watkinson and Hall, 2017) near Lake Matano.

3. Material and methods

3.1. Seismic reflection survey

In 2007 in preparation of the TDP, more than 250 km of high-resolution seismic lines (CHIRP) were acquired with an Edgetech[™] 3200 with SB-424 (Russell and Bijaksana, 2012; Vogel et al., 2015) to characterize the sediment architecture of the basin and identify suitable sites for paleoclimate research. The data were acquired using a length of the source signal of 46 μ s, a frequency of 3–15 kHz, and a shot time interval of 1 s, corresponding to shot spacing of approximately 1.74 m. Coordinates were continuously recorded using a Furano[™] GPS. The data were converted to SEG-Y files that were then imported into the seismo-stratigraphic interpretation software Kingdom 2020 provided by IHS Markit. No bandpass filters were used but small bulk shifts were applied prior to data visualization and export of the seismic sections. The seismic horizons were traced along high-amplitude reflections in the acoustic signals, thus forming virtual lines allowing the definition of different seismic units. Within these units, acoustic facies were identified and described, and their characteristics were associated with specific depositional processes documented in the literature (Adams et al., 2001; Gasperini et al., 2020; Gilli et al., 2004; Maitituerdi et al., 2022; Moernaut and De Batist, 2011; Praet et al., 2017; Sammartini et al., 2021; Schnellmann et al., 2005). Airgun data were also collected to understand basin evolutionary processes and for detailed TDP drill site characterization (Russell et al., 2020b; Russell and Bijaksana, 2012), totalling ~ 1200 km of seismic lines. In this study, airgun data was only used for the generation of a bathymetric map along with the CHIRP data. For details on the generation of the airgun data, we refer to Russell et al. (2020b). For the generation of a bathymetric map, the lake-floor horizon was picked prior to applying a time-depth conversion with a constant acoustic velocity of 1450 m/s for the water column. Interpolation of the seismically-derived lake-floor data was performed in ArcGIS 10.8 using a natural neighbour interpolation method, which resulted in the bathymetric map of Lake Towuti presented here (Fig. 1B).

3.2. Sediment piston-coring

In 2010, the 19.8-m-long Co1230 piston core was collected in ~200 m water depth in the northern Basin A of Lake Towuti (Figs. 1B and 2°42'19"S, 121°35'33"E). The coring site is located a few kilometres downstream of the Mahalona River inlet, towards the distal part of its delta but not directly on the proximal deltaic deposits (Fig. 1). The base of Co1230 is dated to 28.8 cal ka BP (Vogel et al., 2015). The cores IDLE-TOW10-9 B-1K (2°43'12"S, 121°31'32"E; hereafter TOW9) and IDLE-TOW10-6 A-1K (2°43'57"S, 121°30'58"; hereafter TOW6) are 11.5- and 11.2-m-long piston cores recovered from the northern Basin B (Fig. 2) at 154 m and 158 m water depth (Fig. 1B), respectively. The location in the center of the basin distal to the steep slopes and protected from deltaic deposition by bedrock highs results in the deposition of fine-grained, primarily pelagic sediments (Russell et al., 2020b). The base of TOW9 is dated to ~60 ka (Russell et al., 2014). Cores IDLE-TOW10-7 B-1K (2°48'54"S, 121°30'16"E; hereafter TOW7) and IDLE-TOW10-8 B-1K (2°50'40"S, 121°28'03"E; hereafter TOW8), are the only available piston cores from the southern Basins C and D (Figs. 1B and 2). The 11.0-m-long core TOW7 is located in the middle part of the lake at 140 m water depth, between Loeha Island and a bedrock ridge, which splits the southern part into two basins (Basins C and D, Figs. 1 and 2). Core TOW8 (11.2-m-long) was recovered in the deepest part of the southern Basin D at 174 m water depth.

3.3. Petrophysical analyses and radiocarbon dating

Whole core Gamma Ray density (GRAPE) and magnetic susceptibility (MS) measurements were performed on all cores with a resolution of 0.5 cm, using a Geotek Multisensor Core Logger (MSCL) equipped with a Bartington MS2E loop sensor. Split core high-resolution linescan images were brightness corrected using the same parameters for all core sections.

Radiocarbon dates (20 bulk organic carbon and 3 terrestrial macrofossil ages) from Russell et al. (2014) for core TOW9 were projected onto TOW6, TOW7 and TOW8. These projections are based on clearly distinguishable stratigraphic features present in magnetic susceptibility, gamma-ray density data, and changes in lithology at all sites (Fig. 3 and Supplementary Material Fig. S1). Upon transfer of radiocarbon ages, age models were calculated using the IntCal20 calibration curve (Reimer et al., 2020) for cores TOW6, TOW7, and TOW8. The R package CLAM v.2.3.9 (Blaauw, 2010) was used to generate age-depth models using a smooth spline interpolation. For core TOW9 we relied on the age-depth model presented in Russell et al. (2014) and for core Co1230 on the one presented in Vogel et al. (2015).

3.4. Intensity prediction equation

Earthquake intensities in the surroundings of Lake Towuti are only available for strong events. However, a considerable number of smaller earthquakes are located at sufficient distances to reach the shores of the lake with an intensity $\geq VI$. The Intensity Prediction Equation IPE in (Leonard, 2015) was used to estimate the Modified Mercalli Intensity MMI for additional events listed in Supplementary Table S2:

$$MMI = C_0 + C_1 * M_w + C_2 * \ln \left(\sqrt{R^2 + (1 + C_3 * \exp(M_w - 5))^2} \right)$$

where R is the minimum/shortest distance to the shore of Lake Towuti, M_w , the moment magnitude of the event, and C_0 , C_1 , C_2 , and C_3 , are constants, equal to 3.5, 1.05, -1.09, 1.1 respectively.

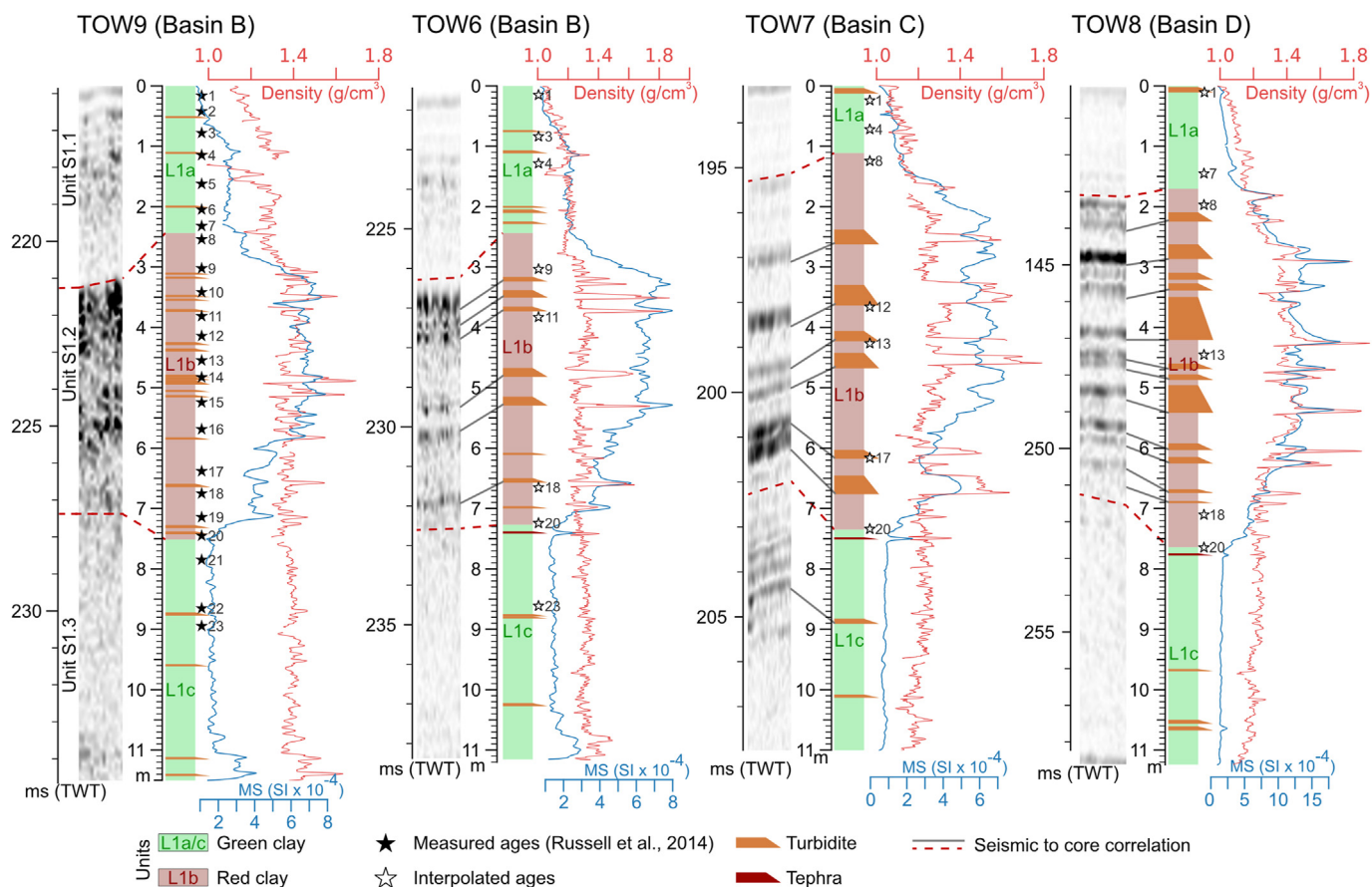


Fig. 3. Core logs (lithological units, turbidites, Gamma ray density and magnetic susceptibility) aligned with respective windows of chirp seismic lines (two-way-travel-time, in ms). Differentiation of green and red clays was done using core images and magnetic susceptibility data. Ages measured on core TOW9 (Russell et al., 2014) are interpolated on the other cores with the matching patterns in MS variations.

4. Results

4.1. Bathymetry

The bathymetric map indicates five basins of variable depth separated transversely by bedrock ridges (Figs. 1 and 4) and fault structures (Fig. 2). The deepest basin to the north (A) receives the majority of direct sediment input from the Mahalona River, which forms a delta that progrades southeastward towards the Basin A center. Owing to its topographic confinement, slopes bordering Basin A are steep, often exceeding $>15^\circ$. The lake-floor morphology of the two Basins B and C is rather flat, with water depths ranging between ~ 120 and ~ 160 m (Fig. 4). Basin B is characterized by gently inclined slopes to the NW and SE, while slopes from the bordering ridges to the N and S are generally steeper, particularly slopes originating off the Loeha Island ($\sim 12^\circ$). Basin C shows a more complex morphology with gradual slopes towards the north and south sills and steepest slopes to the west and east. The southern Basin D is characterized by an expansive relatively flat surface with a nearly constant water depth of ~ 160 m. The slopes bordering Basin D are gently inclined at 3 and 5° along the shoreline but are much steeper (max. 18°) at its northern end, marked by a prominent ridge. Basin E is isolated in the northeast of the lake, featuring a circular shape and a depth of ~ 140 m.

4.2. Seismic stratigraphy

Single and multi-channel airgun seismic data reveal two clearly distinguishable seismic units for Lake Towuti (Russell et al., 2020b). The upper Unit 1, reaching a maximum thickness of nearly 150 m (using a seismic velocity of 1500 m/s) in the southern Basin D, is acoustically well stratified with alternations of parallel and continuous low- and high-amplitude reflections across all basins. The lower Unit 2 varies from ~ 10 to ~ 150 m in thickness and generally shows a chaotic appearance with limited areas of continuous and discontinuous sub-parallel high-amplitude reflections. These two seismic units correlate well with substantial lithological changes in the sediment cores obtained from the 2015 TDP deep drilling boreholes. The sediment succession is comprised of predominantly fine-grained lacustrine sediments in the upper part (Unit 1) and predominantly coarser grained fluvio-lacustrine sediments interspersed with occasional peats in the lower part (Unit 2) (Russell et al., 2020b).

Using the high-resolution CHIRP data, we delineated the seismic stratigraphy of the uppermost strata within Unit 1 into 5 seismic sub-units (youngest Unit S1.1 to oldest S1.5, Table 1, Fig. 4). This sub-classification is based on differences in the amplitude and frequency of reflections (seismic facies) and their overall geometry. However, in the depocenters, where sediment deposits are thickest,

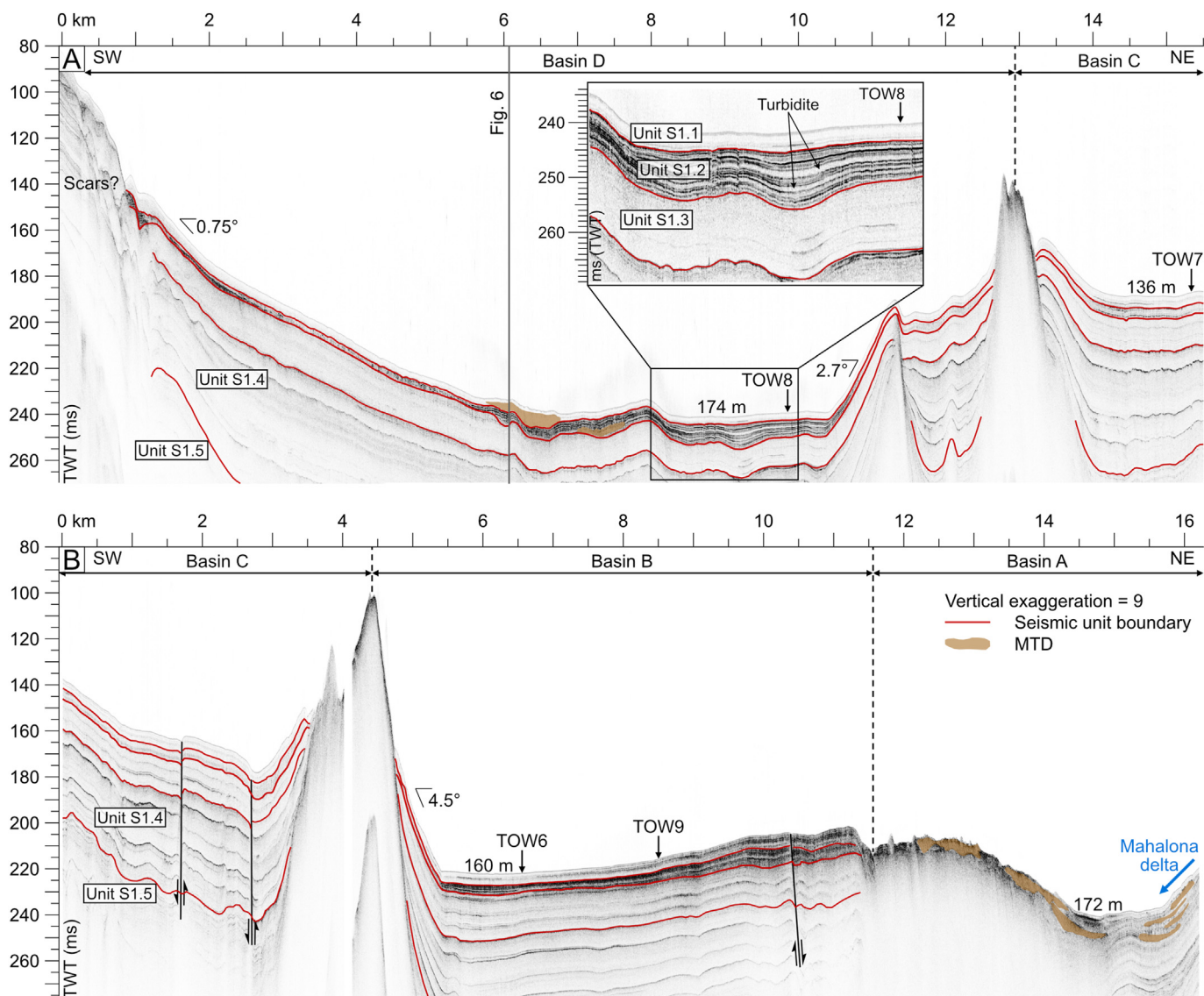


Fig. 4. CHIRP seismic profiles crossing Lake Towuti from southwest to northeast. Core locations are projected onto the seismic sections. See Fig. 1 for locations of cores and seismic sections.

and near the major deltas where coarser sediments prevail, the CHIRP data lack signal strength to image the entire Unit 1 down to the Unit 1/Unit 2 boundary. Correlation of the seismic units between the different basins is not always straightforward as bedrock ridges separate the different basins. In this study, we therefore focus only on the three uppermost seismic sub-units (named Unit S1.1 to S1.3), which are also covered by sediment piston-cores (Fig. 3).

4.2.1. Unit S1.1




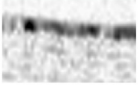

Unit S1.1 reaches an average thickness of 11 ms two-way travel time (TWT, ~8 m using a constant seismic velocity of 1500 m/s, Fig. 4) and is characterized by parallel and continuous reflections, with a general succession of higher amplitudes at the base to lower amplitudes at the top of the unit (Table 1). Some of the reflections terminate in onlaps at the slopes. At sites proximal to the delta, the lower limit of Unit S1.1 is more difficult to determine because gas-rich sediments hamper the visualization of the reflections due to dissipation of energy at depth.

In Basin A, Unit S1.1 is substantially thicker than in the other

basins. This is because steep slopes and the great water depth direct the suspended load from the Mahalona River and its delta towards the Basin A depocenter (Fig. 1, Vogel et al., 2015). The amplitudes of the reflections in this deep basin are weak to moderate, with transparent seismic facies at the base of the slopes. Unit S1.1 in Basin B, which is located farther away and protected by E-W-trending bedrock highs from delta sediments, is much thinner (~5 ms TWT, ~3.5 m) but spread over a large area compared to Basin A. It is acoustically well-stratified, with horizontally continuous and parallel low-to moderate-amplitude reflections over the entire Basin B. In Basin C, Unit S1.1 exhibits a generally constant thickness with parallel and continuous reflections of moderate amplitude (Fig. 4). Its thickness is similar to that in Basin B, except for the western littoral part where it tends to become thinner. The reflections of Unit S1.1 in Basin D are parallel and continuous with low amplitudes and an average thickness of 3 ms TWT (~2.3 m). A few thick and acoustically transparent acoustic strata, identified as MTDs are locally identifiable, especially towards the northwestern shore of the basin.

Table 1

Description of CHIRP seismic units of Lake Towuti with respective thicknesses in different basins A-D using a constant seismic velocity of 1500 m/s for time-depth conversion.

Unit	preview (Basin D)	description	maximal thickness			
			A	B	C	D
S1.1		Parallel, continuous, high-(base) to low-amplitude (surface) in Basin A. Acoustically well-stratified, with horizontally continuous and parallel reflections in Basins B, C and D	8 m	3.5 m	3.5 m	2 m
S1.2		High-amplitude, continuous and sub-parallel in Basin A. Succession of acoustically high-amplitude, parallel, continuous and homogeneous reflections in Basin B. Medium- to high-amplitude, semi-continuous, with ruptures (irregularities and discontinuities) in Basin C. Medium- to high-amplitude, continuous and parallel in Basin D	Undefined (loss of energy)	3.5 m	4.5	8.25 m
S1.3		Not imaged in Basin A. Thinly acoustically alternated reflections of low- and very low-amplitude, with high frequency, globally homogeneous and continuous, parallel with some minor deformation and disruption in Basin B, C and D		12 m	10.5 m	9.5 m
S1.4		Several high-amplitude reflections associated to tephra layers (Russell et al., 2020a, 2020b). Parallel and sub-parallel disrupted low-amplitude reflections in Basins B, C and D		35	20 m	33 m
S1.5		Succession of acoustically low- to very low-amplitude reflections, parallel and sub-parallel, continuous and homogeneous in Basin B, C and D			Undefined (loss of energy)	

4.2.2. Unit S1.2

The boundary between Units S1.1 and S1.2 is defined by a high-amplitude reflection visible across almost the entire sedimentary subsurface of Lake Towuti. This reflection is the first of a succession of high-amplitude reflections, which together form Unit S1.2 (Table 1). In the deep Basin A, the lower boundary of Unit S1.2 is not visible on the CHIRP data, but the thickness reaches at least 14 m (~19 ms TWT) in the deeper part. Unit S1.2 reflections are high in amplitude in the upper part, but appear less pronounced in the lower parts likely due to energy dissipation with depth. The decimetre-scale high- and low-amplitude alternations are continuous and sub-parallel. Variation in thickness is observed, with divergent stratification in the southern part of the Basin A depocenter. Most reflections terminate with onlaps onto frontally emergent subaquatic landslides at the toe of the slopes. Unit S1.2 is not visible in the CHIRP data in proximity to the Mahalona River delta (Fig. 4).

In Basin B, Unit S1.2 is comparably thin (~5 ms TWT, ~3.5 m) with ~8 clearly discernible, continuous, homogeneous, and high-amplitude reflections. The alterations become less distinct in the depocenter located to the north of the Loeha Island and are interspersed with acoustically transparent facies of varying thicknesses. To the east of this basin, chaotic facies appear with some reflections preserved close to the shoreline (Fig. 5), identified as a MTD.

Unit S1.2 in Basin C appears less continuous and is relatively thin. Some medium- to high-amplitude reflections are parallel over longer distances, but often show discontinuous reflection patterns with irregularities (Fig. 4). These patterns occur in particular in the eastern part of Basin C, where a thick (up to 12 ms TWT, ~9 m) megaturbidite covering a large area is observed, increasing the thickness of the unit to 25 ms TWT or almost 18 m (Supplementary Material Fig. S2).

The reflections in Unit S1.2 in Basin D show medium- to high-amplitudes and are generally continuous and parallel. Within this unit, several alternations of high-amplitude reflections and transparent seismic strata occur. Although the packages of high-amplitude reflections are of nearly uniform thickness in this

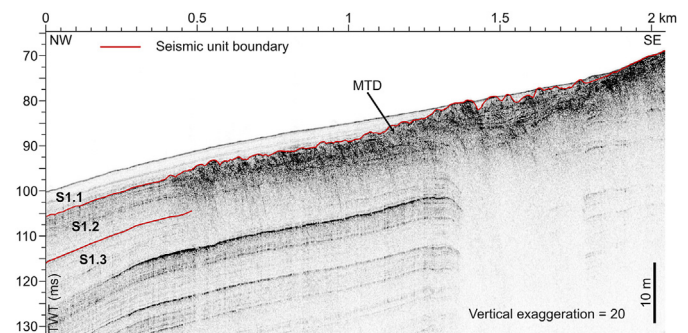


Fig. 5. NW to SE CHIRP seismic profile close to the eastern shoreline of Basin B, showing a large MTD with an irregular surface.

basin, the transparent strata pinch out towards the shorelines and increase in thickness towards the basin center to ~1 m. Medium-amplitude reflections appear very locally, sometimes with identifiable geometric structures, thickening in the center, with onlap terminations, transparent and with a very irregular surface (Fig. 6).

4.2.3. Unit S1.3

Similar to the transition from Unit S1.1 to S1.2, the boundary between Units S1.2 and S1.3 is marked by a strong contrast in reflection amplitude with the lowest high-amplitude reflection marking the unit boundary. Unit S1.3 is characterized by thinly-spaced reflections with amplitudes lower than those in unit S1.2. In Basin A, Unit S1.3 is not imaged by CHIRP data due to limited acoustic penetration. In Basins B, C, and D, it is homogeneous with thicknesses of ~16, 14 and 13 ms TWT (~11, 10, and ~9 m), respectively. The reflections are of low- to very low-amplitude (Table 1), they are continuous across the basins, parallel and show only minor undulations. Within Basins B and C, two groups of medium-amplitude and evenly-spaced reflections are observable. These two groups appear as a single strong reflector in Basin D.

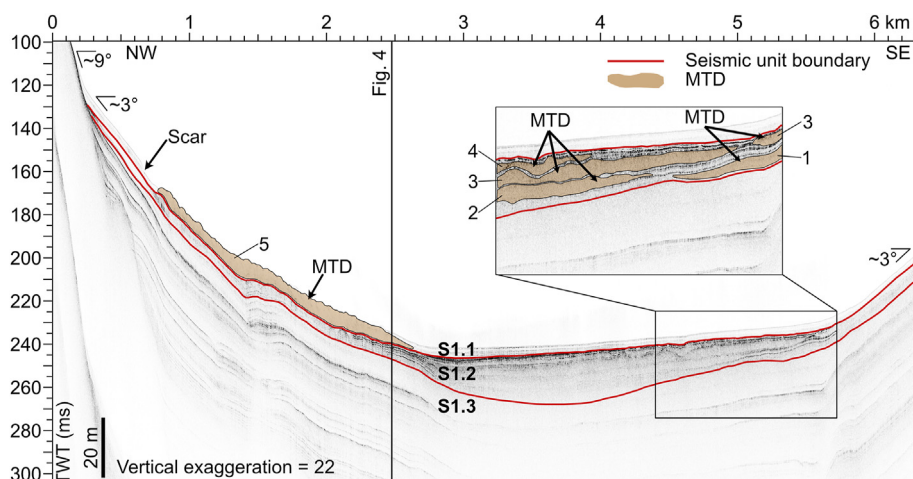


Fig. 6. NW to SE CHIRP seismic profile through the depocenter of Basin D (see Fig. 1 for location). Seismic unit boundaries for S1.1 to S1.2, and S1.2 to S1.3 are delineated by the red lines. The MTDs, triggered on opposing slopes of the lake, are highlighted in brown. The numbers 1 to 5 correspond to the succession of MTDs from the oldest (1) to the youngest (5).

4.2.4. Units S1.4 and S1.5

Unit S1.4 is bounded at the top with a strong reflector. It is thick (~70 ms TWT, ~50 m) and widely transparent, including several high-amplitude reflections, associated with cm-to dm-thick tephra layers (Russell et al., 2020b). Unit S1.5 begins at its top with a higher number of discernible reflections of low-to very low-amplitudes, probably caused by the loss of energy with depth due to geometric spreading. These two units are characterized by parallel and sub-parallel and often non-continuous reflections (Table 1).

4.3. Lithostratigraphy of sediment cores

Sediment cores recovered from Lake Towuti's deeper basins show lithologies dominated by fine-grained pelagic muds with variable but generally low contents of organic matter and siderite (Russell et al., 2020b). Classifications introduced by Russell et al. (2014, 2020b) and Vogel et al. (2015) comprise alternations of green organic matter-rich and reddish sideritic clays. These alternations are a result of climate-induced changes in water-column oxygenation and lake level with the reddish-sideritic clays being deposited during colder and drier climates (glacials, stadials) with lake-level lowstands and deep oxygenation of the water column. In contrast, green clays are deposits that formed during wetter and warmer climate conditions (interglacials, interstadials) with lake-level highstands and a stratified partly anoxic water column (Russell et al., 2020b).

The fine-grained muds are occasionally interrupted by turbidites, consisting of coarser-grained beds with a characteristic coarse-grained/sand-sized normal graded base overlain by a more homogenous silt-dominated succession occasionally showing cross-bedding towards the top and typically capped by a several millimetre-thick clay bed (Fig. 7). The coarse base of these layers has grain sizes >100 μm and is clearly distinguishable from surrounding sediments by high GRAPE values (Figs. 3 and 7). We attribute the occurrence of abundant plant macrofossils, mainly occurring in the homogenous silt-sized sequence of some turbidites, to be a source indicator for deltaic material. Hence, these types of turbidites are very numerous in the deep Basin A where they have been described in detail and have been assigned to seismically triggered Mahalona Delta slope collapses (Vogel et al., 2015). We also find these features in the turbidites deposited at the TOW 7 site, where they probably originate from the slopes of the Loeha Delta. Turbidites lacking abundant plant macrofossils,

which represent the majority at distal coring sites, are likely originating from mass wasting of hemipelagic slopes that experience little direct river sediment deposition. Color differences of the coarse base and the upper homogenous turbidite succession are likely the result of bedrock differences in sediment-source areas. The Mahalona River primarily delivers sediments with abundant serpentine minerals (Morlock et al., 2019; Vogel et al., 2015) explaining the dark-green colored base of these turbidites. In contrary, sediments supplied by the Loeha River show a more felsic composition (Morlock et al., 2019) likely leading to the lighter colored sediments in turbidites at site TOW 7 (Fig. 7).

Here we introduce a new and detailed account of turbidite occurrence, thickness, and chronological context (Fig. 3) in the form of a Towuti turbidite catalogue (Supplementary Material Table S1). Centimeter to decimeter-thick turbidites are abundant across the entire lake but most common in the deep Basin A (Co1230) in which units L1a and L1b are predominantly composed of these beds (Vogel et al., 2015). Basins B–D show substantially fewer turbidites, especially within Unit L1a. Overall, 23 turbidites were observed in core TOW9 (Basin B), with an average thickness of 3.1 cm (from 1 to 5 cm). Cores TOW6 (basin B) and TOW8 (Basin D) comprise 16 turbidites each, but the average thickness is 4 cm in TOW6 and 16 cm in TOW8. In core TOW7 (Basin C), only 9 turbidites are observed with an average thickness of 15.5 cm.

Alternations coinciding with the occurrence of green or red-sideritic clays are present across all petrophysical and geochemical datasets obtained for cores from Lake Towuti including TOW6, 7, 8, and 9 (Fig. 3) as well as Co1230 (Vogel et al., 2015). Based on these major changes in lithology we suggest a sub-unit classification scheme for the upper ~10 m in the piston cores, based on the seismic and lithological unit classification introduced by Russell et al. (2020b). For the purpose of correlating lithologies between the different basins and for core-to-seismic correlation, we rely mostly on the MS and GRAPE data. MS is elevated in red sideritic clay and low in the green clay lithologies (Tamuntuan et al., 2015). MS therefore serves as an ideal dataset to correlate lithologies between the different cores and basins. GRAPE is particularly elevated in coarser/denser lithologies but also shows subtle changes at the transition of the fine-grained pelagic lithologies due to differences in sedimentary iron contents and interspersed sandy layers, often observed at the base of turbidites. GRAPE therefore serves as an ideal dataset to correlate turbidites between core and seismic data.

Three lithostratigraphic Units L1a, L1b and L1c can be identified

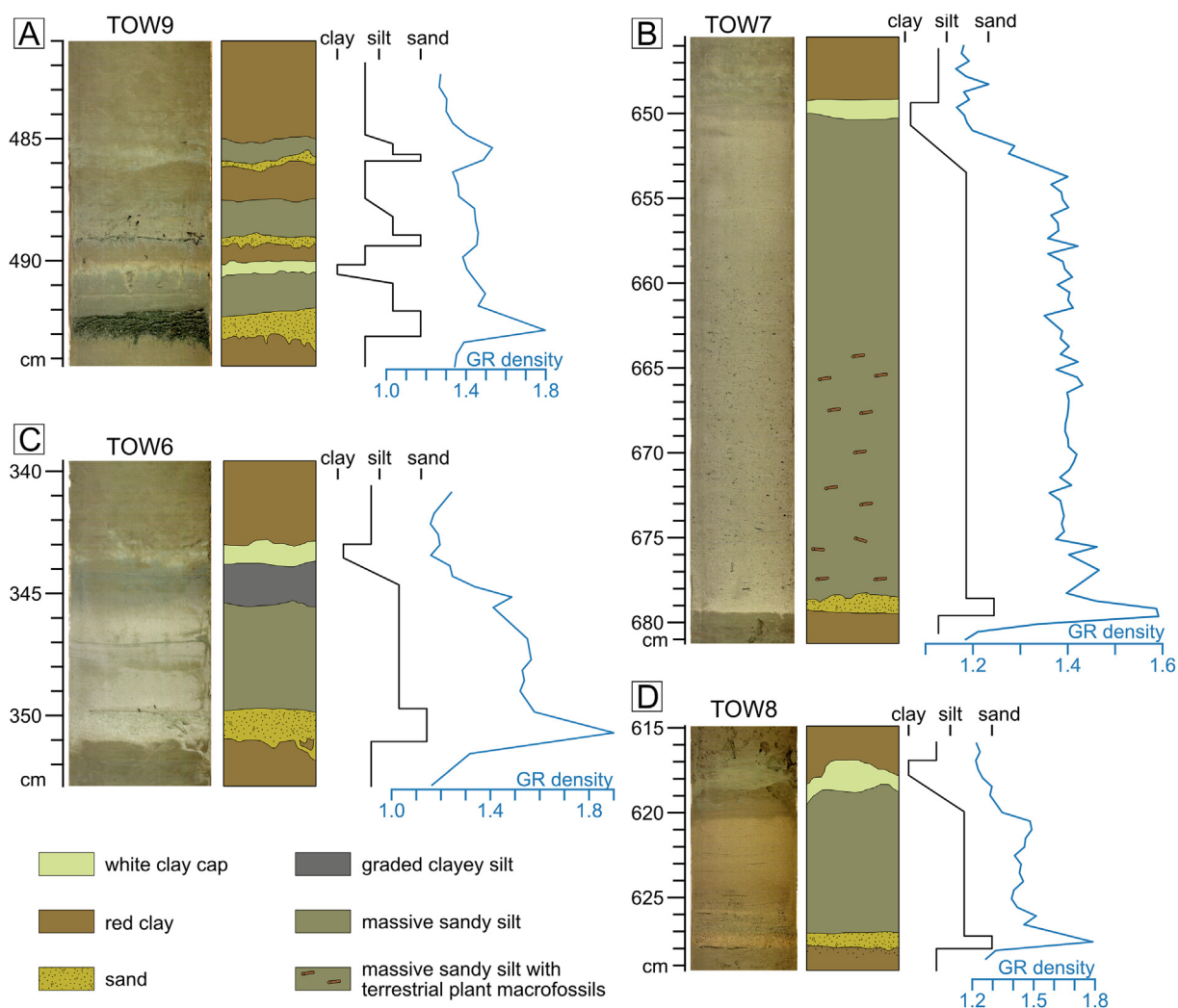


Fig. 7. Core section images with lithological and petrophysical characteristics of typical turbidites observed in the cores.

and correlated between cores TOW6, TOW7, TOW8, and TOW9 based on visual appearance and by matching prominent features of the MS data. The thickness of Unit L1a ranges from 113 (TOW7) to 240 cm (TOW9) in Basins B, C, and D, and reaches 640 cm thickness in the deep Basin A (TOW4 and Co1230). Unit L1a is composed of light green clay interspersed with cm-thick brownish to dark green beds. MS data shows some variability in Unit L1a but values are relatively low. One remarkable feature of Unit L1a, present in all the cores from the different basins, is a 7–17-cm-thick deposit characterized by a massive mottled siderite-bearing silty clay with elevated GRAPE values at the transition to Unit L1b, likely related to sediment remobilisation from onshore slopes induced by the lake-level rise and subsequent formation of siderite concretions (Vuillemin et al., 2019). Unit L1b has a relatively constant thickness across the entire lake (between 506 and 622 cm). This unit is composed mainly of light to dark brownish red clay, sometimes tending towards light orange-red. MS variability is strong with high average values ($>3 \text{ SI } 10^{-4}$). Unit L1c is the lowermost identifiable lithologic unit in the piston cores. Its total thickness cannot be determined because the unit was not sampled entirely in the piston cores. The description provided here is based on the upper ~3 m of this unit collected in the piston cores. Unit L1c is composed of dark green clay interspersed with lighter colored clay. This unit is well-structured with bedding in the mm – cm range.

This new unit and event deposit framework in combination with the projected chronology allows us to construct a depositional and event history of Twotwi's different basins. The three lithological units (L1a–L1c) can be discerned in all piston cores from Basins B, C, and D. The boundary between Units L1a and L1b is dated to $\sim 12.3 \pm 0.13 \text{ ka}$ and the transition between Units L1b and L1c is dated to $\sim 40.8 \pm 0.64 \text{ ka}$. In unit L1c MS-based core-to-core correlation is hampered by the muted data variability and the lack of reliable radiocarbon dates in cores TOW 7 and 8. Sedimentation in Unit L1c appears fairly constant with estimated rates of up to 15 cm/ka in all of the sediment cores. Therefore, we here focus on the last ~40 kyr BP where chronological constraints are most robust also due to the identified tephra marker layer, clearly visible in cores TOW6, TOW7 and TOW8, and dated to ~41 ka (Fig. 3). Sedimentation rates, calculated by considering turbidites as instantaneous (constant ages), vary between lithological units and cores from different basins. In contrast, Unit L1b shows a variable sedimentation rate, with a prominent peak in all cores but particularly pronounced in TOW9 with 35 cm/ka around 560 cm (~28.8 ka) and TOW7 with 38 cm/ka at 325 cm (~21 ka). This increase in sedimentation rate in the Unit L1b red clays is followed by a slight decline and stabilization at 10–20 cm/ka towards the top of Unit L1a (Fig. 8) in all cores.

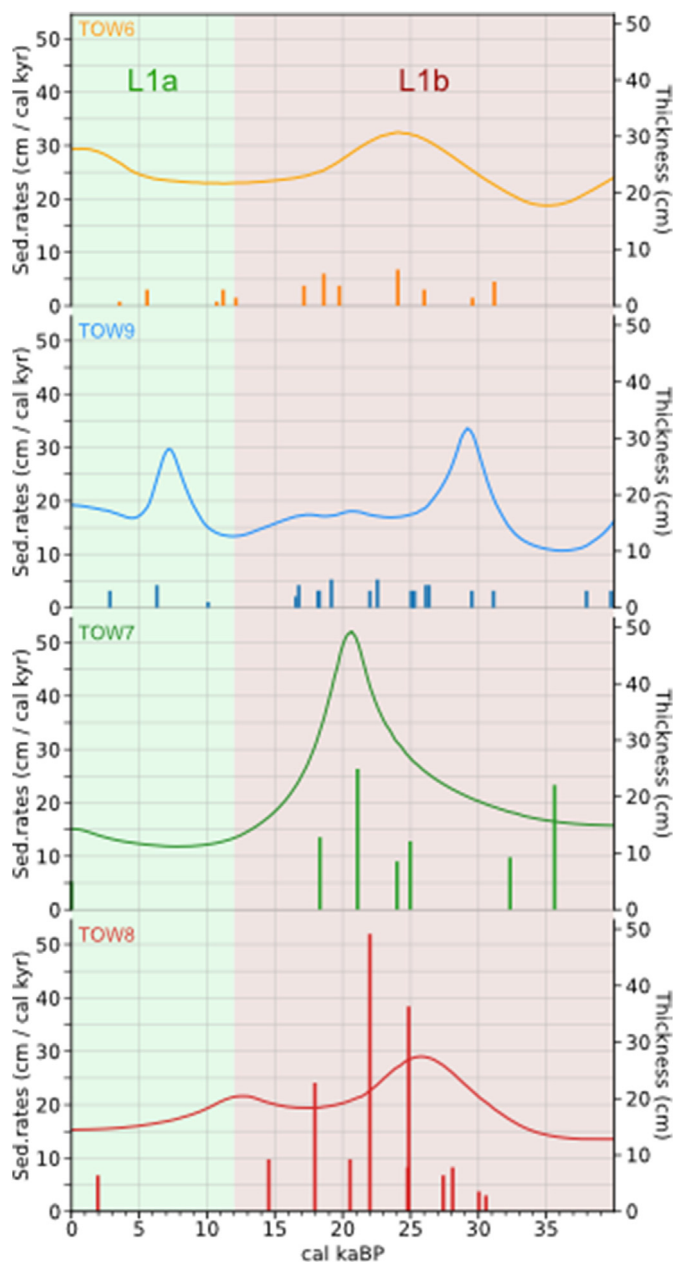


Fig. 8. Comparison of event free sedimentation rates (curves) and turbidite thicknesses (bars, in cm) on cores TOW6 and TOW9 (Basin B), TOW7 (Basin C) and TOW8 (Basin D). For visual purposes, these data are based on smoothed age models. The data are plotted for the last 40 kyrs due to extrapolations beyond that time interval being not very coherent.

Of all the turbidites recorded in the cores, more than half occur in the red clay Unit L1b. Both the abundance and thickness of turbidites (Fig. 9) is increased between ~10 and ~35 ka relative to preceding and following periods. Turbidites constitute between 10.4% (TOW9) and 41% (TOW8) of the entire Unit L1b succession. The thickness of background sediments not including turbidites of Unit L1b differs between the basins (Table 2) with 348 cm in Basin D (core TOW8), 457 cm (core TOW9) and 429 cm (core TOW6) in Basin B, and 486 cm (core TOW7) in Basin C. Therefore, a significant overall increase in sedimentation rate in the red clays in Basin C relative to the other basins and in particular to Basin D is observed.

4.4. Sediment core-to-seismic correlation

In general, a strong correspondence between lithological and seismic facies is observed. This is particularly well demonstrated by the strong relationship of density with amplitude changes in seismic reflection data (Fig. 3). Low-amplitude reflections in seismic Unit S1.1 coincide well with lithologic Unit L1a, which is characterized by green clays and infrequent occurrence of coarser turbidites or MTDs, as is also evident by the overall low density. Likewise, the transition between seismic Units S1.1 and S1.2 coincides with the lithological Unit L1a to L1b transition as it is characterized by an increase in amplitude and sediment density, respectively. Individual turbidites are clearly resolved in seismic data for cores TOW6, 7, and 8 where these deposits reach thicknesses of several decimetres. On the contrary, turbidite thickness in TOW 9 is not sufficient to provide a clear distinction between individual deposits in seismic data but the increase in turbidite frequency leads to an overall increase in sediment density and thereby seismic reflection amplitude. A sudden decrease in seismic reflection amplitude marks the seismic Unit S1.2 to S1.3 transition and matches broadly with the change in lithology from high-density red clays of lithologic Unit L1b to lower density green clays of Unit L1c. Thick turbidites creating high-amplitude reflections in seismic data are largely absent in Units S1.3/L1c.

5. Discussion

5.1. Interpretations on sediment thicknesses

The thickness of seismic and lithologic units differs greatly between the basins. Lithological Units L1a and L1b in Basin A are 3–6 times thicker than in the other basins of the lake. The Mahalona River leads to a significant discharge of sediment directed primarily towards the deep Basin A (Costa et al., 2015; Hasberg et al., 2019; Morlock et al., 2019; Vogel et al., 2015), and the slopes surrounding the basin are steep with angles reaching up to 30°. This morphology results in an effective trap for sediments supplied by the Mahalona River (Vogel et al., 2015). Notable spatial variations in thickness are also observed elsewhere in the lake, albeit with much smaller magnitudes. Lithological Unit L1a is relatively thin in Basin D (~170 cm) and very thin in Basin C (~110 cm) compared to Basin B (~240 cm, Figs. 3 and 4). We interpret these thickness variations of Unit L1a primarily as a result of spatial differences in sediment supply from rivers and by basin proximity to the Mahalona River inlet, which is the main source of suspended sediment loads to the entire lake but particularly to Basins A and B. In contrast, the southern Basins C and D receive sediment supply by smaller rivers with the largest being the Loeha River entering Basin C (Figs. 1 and 2). However, the sediment input from the Loeha River is probably, to a large extent, also diverted to the northern basins by the Loeha island and the associated NW – SE trending bedrock ridge (Fig. 1B) clearly visible in the bathymetric data. Additional submerged bedrock ridges surrounding Basin C also contribute to a lower thickness of Unit L1a in this southern basin.

5.2. Earthquakes as triggers of slope failure in Lake Towuti

Available data for recent earthquakes on Sulawesi and more specifically for the vicinity of Lake Towuti, based on the USGS (Shakemap by USGS Earthquake Hazards Program; <https://earthquake.usgs.gov/earthquakes/eventpage/usp000huje/shakemap/intensity>) and IPE show 12 earthquakes with MMI \geq VI (Supplementary Material Table S2), sufficient to trigger

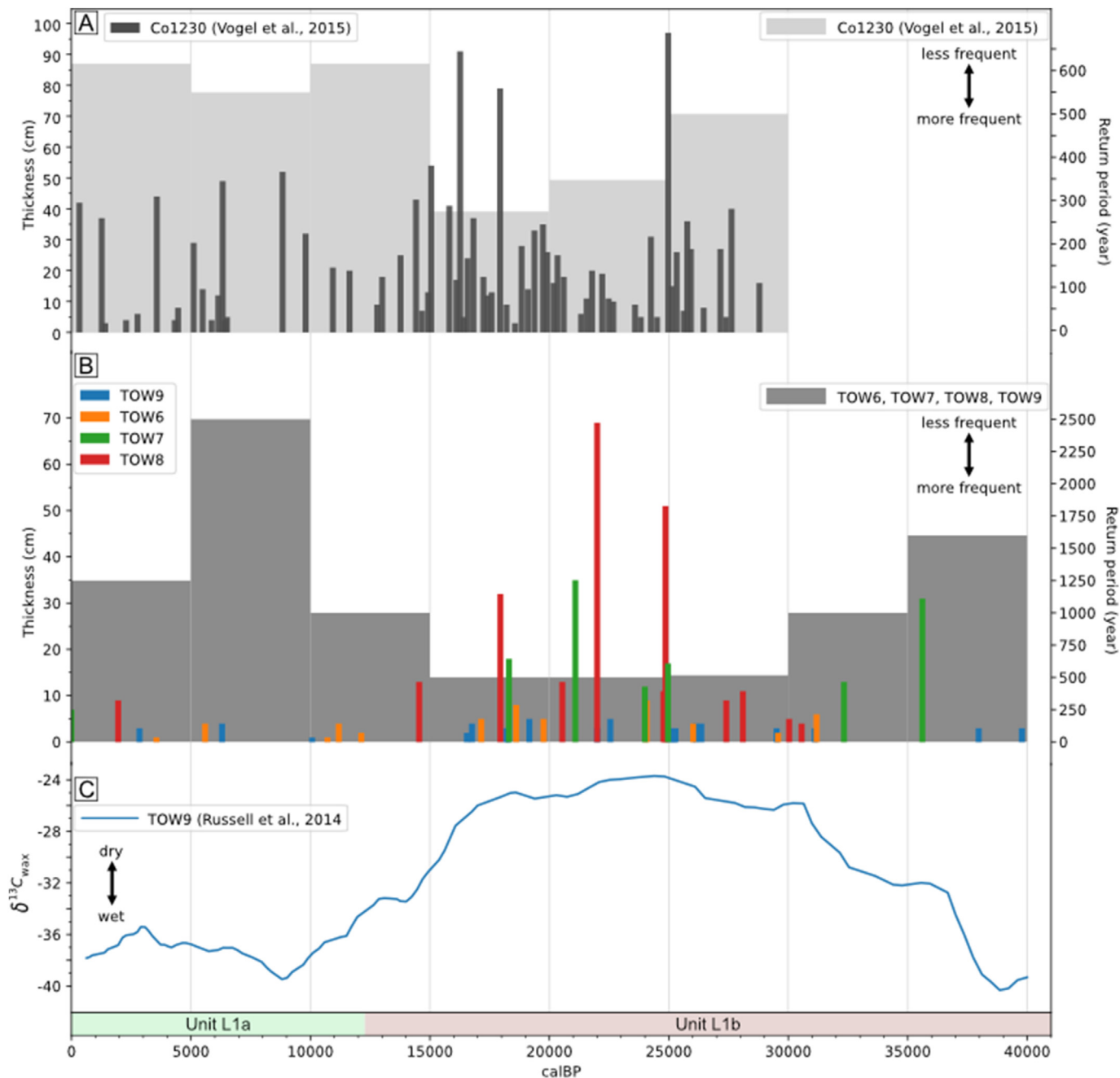


Fig. 9. (A) Turbidite thicknesses and 5 kyrs interval return periods of core Co1230 in Basin A (Vogel et al., 2015) and (B) for each core of this study in Basins B, C and D. (C) Comparison with leaf wax $\delta^{13}C$ climate proxy data indicating regional changes in hydroclimate and associated vegetation cover and structure (Russell et al., 2014).

Table 2

Comparison of lithostratigraphic Unit L1b thicknesses with and without turbidites. The turbidite proportion is relative to entire Unit L1b (100%).

Thickness Unit L1b (cm)	TOW9 - Basin B	TOW6 - Basin B	TOW7 - Basin C	TOW8 - Basin D
with turbidites	510	484	623	592
without turbidites	457	429	486	348
turbidite proportion (% Unit L1b)	10.4	11.4	22	41.2

sublacustrine slope failures (Moernaut et al., 2007; Van Daele et al., 2015). As an example, the 2011 Mw 6.1 earthquake with its epicenter 18 km to the north of Lake Towuti along the MF induced ground shaking with an intensity of VI along Towuti's northern shore (Fig. 2). In 1941, a Mw 6.2 earthquake was recorded with an

epicenter 8 km to the southeast of Lake Towuti, with an estimated MMI intensity of VII calculated on the shoreline. We suggest that this event is responsible for the surficial MTD deposited on the western slope in the southern Basin D (Fig. 6). Basinward, the MTD is associated with a moderate-to high-amplitude surface reflection

caused by the deposition of coarse material in a turbidite. This 4 cm thick turbidite is recovered in core TOW8, only 1 cm below the sediment-water interface (Supplementary Material Fig. S3). A more robust age determination using for example short-lived radionuclides is hampered by the extremely low sedimentation rate of around 0.1 mm per year. Nevertheless, we suggest that this deposit is a potential candidate for mass wasting related to the 1941 earthquake (Supplementary Material Fig. S3) when applying the above-mentioned sedimentation rate.

To better assess the return periods of earthquakes causing macroseismic intensities $\geq VI$ and $\geq VII$ at the lake shore we used the IPE (Leonard, 2015) and earthquake events with $M_w \geq 4.5$ from the ISC catalogue, 2021. These data suggest return periods of ~ 8 years for $\geq VI$ and ~ 32 years for $\geq VII$ intensities, based on 12 events covering the last 100 years (Supplementary Material Table S2). However, turbidites recorded in the cores of Lake Towuti are far less frequent compared to the number of earthquakes that can generate intensities $\geq VI$ at Lake Towuti. This is likely a result of insufficient sensitivity at Lake Towuti to record each individual seismic event with a triggered slope instability due to the overall low sedimentation rate in the different basins.

Before interpreting the seismic origin of turbidites, potential hydrological events must be excluded. An earthquake can cause destabilization of a slope, triggering a mass movement that will transition into a turbidity current (Kremer et al., 2017; Sabatier et al., 2022). In contrary, heavy precipitation induced processes such as floods and mudstreams (Wils et al., 2021a) cause a more steady flow of suspended sediment into the lake at the river mouths, inducing an increase in the capacity to erode and transport sediment along its path (Wilhelm et al., 2022). Many studies have focused on discerning earthquake- and flood-triggered turbidites (Kremer et al., 2015; Lauterbach et al., 2012; Praet et al., 2020; Vandekerkhove et al., 2020). Typically a sharp coarse-grained base overlain by a fining upward section is characteristic of turbidites related to a rapidly increasing energy, such as floods, spontaneous slope failure, or earthquake-induced slope failure (Sabatier et al., 2022; Talling, 2021; Vandekerkhove et al., 2020; Wilhelm et al., 2017). Flood-generated turbidites are often characterized by angular-shaped grains and often show several normal graded intervals and sometimes also reverse grading in one event as a result of changes in runoff volumes during flooding and a generally prolonged period (hours-days) of peak flow (St-Onge et al., 2004; Sturm and Matter, 1978; Vogel et al., 2015; Wilhelm et al., 2017). On the contrary, turbidites originating from slope failures typically show a normal graded base immediately followed by a thick and more homogenous sediment succession with an overlying clay cap as a result of the mobilization and fluidization of a large volume of sediment in a short time (Beck, 2009; Vandekerkhove et al., 2020). Sediment components such as abundant macrofossils are often indicative for a riverine source but are not suitable to differentiate between flood versus delta slope-failure sourced turbidites because macrofossils would also be mobilized and deposited in primarily riverine-sourced delta sediments. Based on their broadly basin-wide consistent characteristic features with a graded coarse-grained base followed by a homogenous succession sometimes showing cross-bedding towards the top and a clay cap in combination with frequent large magnitude earthquakes in the region, we follow the interpretation by Vogel et al. (2015) suggesting turbidites in Towuti originate primarily from earthquake-triggered and slope-failure-induced mass-movement processes. The absence of flood turbidites at the coring sites studied here can be explained by the morphology of the lake that constrains the propagation of flood-generated underflows and turbidity currents from the major inlets (Russell et al., 2020b). Several ridges in Towuti

constitute effective hydrologic obstacles, especially in Basins B and D (Fig. 1), where the sediment input from rivers is already quite low.

Mass movements occur when the gravitational force exerted on the slope sediments exceeds their resisting force. This balance is influenced by several parameters, such as slope inclination (Sultan et al., 2004), sediment thickness and sedimentation rate (Wilhelm et al., 2016), gas hydrate destabilization (Haq, 1998), pore pressures (Urlaub et al., 2015) and existence of weak layers (Strupler et al., 2017). Gas-hydrate stability, pore-pressure changes and activation of weak layers can be affected by seismic shaking contributing to slope instability and failure. For example, during an earthquake and the associated ground motions, pore-water escape can induce large-scale sediment liquefaction or pore-water overpressure, thereby reducing the sediment's shear strength (Biscontin et al., 2004). While spontaneous subaquatic or rainfall-induced onshore slope failures cannot be ruled out completely, we suggest these to be rather rare events considering the low sedimentation rates leading to slow slope charging in combination with frequent seismic shaking. Frequent seismic shaking may, in addition, also lead to so-called seismic strengthening through enhanced sediment compaction and efficient removal of surficial sediments (Molenaar et al., 2019).

The major parameters that control the formation of a turbidite triggered by an earthquake are the slope angle, the thickness and geotechnical properties of the sediment package emplaced on the slope, as well as the intensity of the seismic shaking (Lee et al., 1996; Molenaar et al., 2021). The slope angle as well as the thickness of the sediment package and its rheology are factors determining the stability of the sediments and thus the sensitivity to generate a failure (Hansen et al., 2016; Strasser et al., 2007, 2011; Van Daele et al., 2015; Wiemer et al., 2015; Wilhelm et al., 2016). In case of Basin A with a high supply of suspended sediments from the Mahalona River, we assume that the slope angles and the sediment package are rather sensitive to seismic shaking as witnessed by a larger number of turbidites compared to the other basins (Russell et al., 2020b; Vogel et al., 2015). However, turbidite return periods of >200 years in Basin A are still well below the return periods of earthquakes leading to intensities of $\geq VI$ and $\geq VII$ (Supplementary Material Fig. S4). The slopes in Basin B originating from the Loeha Island are similarly steep, with up to 10° in areas where mass movements occur (Supplementary Material Fig. S5) but lack the steady supply of sediment from major rivers. This is emphasized by the presence of frequent but rather thin turbidites at coring sites TOW6 and TOW9. In contrast, slopes are generally much more gently inclined in the southern Basins C and D ($<4^\circ$). This permits accumulation of a thicker sediment package over time that is less prone to failure. Turbidites in the southern basins are consequently less frequent but generally thicker than in Basin B (Figs. 3 and 9B), as also evidenced by the presence of large slope failure related MTD's observed on seismic data (Fig. 6). Hence, the less frequent but thick turbidites suggest a lower sensitivity of slopes to fail during moderate earthquakes, and therefore imply a lower sensitivity to ground shaking. Consequently, we propose that high-intensity shaking is required to cause slope failures in the southern Towuti basins. We suggest that such strong events must have triggered the large MTDs clearly visible in seismic units S1.1 and S1.2 and in cores TOW7 and TOW8. In Basin D, several MTDs are recorded on the CHIRP data, including some deposits within Unit S1.2 that appear to have been generated during the same event but on different/opposing slopes (Fig. 6 and Supplementary Material Fig. S6) thereby fulfilling the synchronicity criterium for an earthquake trigger as suggested by Schnellmann et al. (2002).

Owing to the ridges separating the basins, hampering the tracing of individual reflections, and age uncertainties, correlation

of individual turbidites in the different basins remains rather vague. Dating these turbidites to estimate the age of an earthquake is very challenging, as radiocarbon dates are extrapolated from TOW9 and errors often exceed the recurrence intervals of major events (Talling, 2021). Nevertheless, the general increase in occurrence of turbidites in Unit L1b (Figs. 3 and 9 B–C) clearly shows increased mass-movement activity during the dry Last Glacial between ~15 and 30 ka at Lake Towuti. This pattern suggests a potential aseismic influence related to regional changes in hydroclimate and Lake Towuti's associated lake level on the sensitivity towards seismic triggering of MTDs.

5.3. Climate-induced changes in sensitivity of slope failures

Based on previous studies in different settings, the link between lake or sea-level changes with the frequency of subaqueous mass failures has raised a controversial and ongoing debate. Some studies conclude that an increase in slope sensitivity towards failure occurs during a highstand phase (Brothers et al., 2013; Lu et al., 2021a; Neves et al., 2016) due to higher sedimentation rates, as well as due to immersion of steep banks, which destabilize the cohesion of sediments when they are loose and/or coarse. On the contrary, other studies report an increase in slope failures during lowstands due to the (i) more significant erosion of emerged shelves resulting in higher sedimentation rates on the slopes (McHugh et al., 2002) eventually leading to sediment overloading and decreasing slope stability; and/or (ii) lowstand-induced pore-fluid overpressure (Anselmetti et al., 2009; Blumberg et al., 2008; Lee et al., 1996) possibly closely restricted to the phase when the lake-level is dropping (Moernaut et al., 2010). A higher frequency of turbidite deposition in the late Pleistocene and a lower frequency during the Holocene was observed at all latitudes (Anselmetti et al., 2009; Blumberg et al., 2008; Brothers et al., 2013; Lee et al., 1996; Wien et al., 2006) similar to Lake Towuti. Despite the discrepancies between high and low water levels, it seems evident that slope stability is influenced strongly by climate-induced water-level changes.

Our study of Lake Towuti turbidite occurrence indicates increased slope sensitivity towards failure during a climatically driven lake-level lowstand (Fig. 9). Indeed, the difference in turbidite occurrence between Units L1a and L1b is probably not associated with a change in tectonic activity alone. Previous studies suggest changes in lithology to be related with changes in the regions hydroclimate with green clays (L1a) deposited during warm and humid periods, and red sideritic clays (L1b) during colder and drier climate conditions of MIS 2 (Konecky et al., 2016; Russell et al., 2014) with lower lake levels (Vogel et al., 2015) and deep mixing at Towuti (Costa et al., 2015). Accordingly, deposition of the green clays of L1a (~Holocene) and L1c (MIS 3) took place under lake-level highstands and a permanently stratified water column with anoxia in bottom waters (Russell et al., 2020b). We suggest the increase in turbidites in L1b to be related to changes in the regions hydroclimate (Konecky et al., 2016; Russell et al., 2014; Wicaksono et al., 2017) and an associated up to 30 m lower lake-level (Vogel et al., 2015) between ~29 and 15 kyr BP, coincident with the regionally drier last glacial. Although an overall drier climate does not rule out heavy precipitation events and increased flooding, the observed turbidite compositions at our distal coring sites do not indicate increased occurrences of flood-related turbidites. However, accumulation of sediment in the catchment in intermediate storages/sinks that can be mobilized during single heavy precipitation events in combination with a change in style of erosion during dry phases (Morlock et al., 2019) may also contribute to rapid slope charging and thereby a higher susceptibility of slopes to fail during an earthquake.

Lake-level changes in Lake Towuti also affected the background sedimentation rate, a parameter that was already shown to play a considerable role in the occurrence of MTDs in other basins (Leynaud et al., 2007; Owen et al., 2007). In fact, all cores recovered from Lake Towuti's different depocenters show almost a twofold increase in background sedimentation rates during the last glacial period between ~41 and 15 ka BP (Fig. 8). The increase cannot be explained by the coincident changes in sediment composition alone with more abundant diagenetic siderite in glacial red clays compared to more organic-rich interglacial green clays (Russell et al., 2020b). While sedimentation rates in Towuti's depocenters remain relatively low overall, we suggest lowstand-forced sediment redeposition from the exposed shore and shelf areas to be the most important factor explaining the increase in event-free sedimentation rate. Slope-to-basin focusing is also supported by rather constant glacial-interglacial slope sedimentation rates relative to the substantially higher glacial versus interglacial sedimentation rates in the depocenters. In addition, the lowering in base level of the tributaries likely contributed to increased sediment redeposition by rivers eroding into their own delta deposits (Morlock et al., 2019; Vogel et al., 2015). Moreover, the discharge of river suspension moved lakeward and focused closer to the basin depocenters. We thus hypothesize that the lowstand-forced increase in sediment redeposition caused a notable increase in slope charging that, in turn, increased the susceptibility of slopes to fail due to seismic shaking. Seismic data, acquired to image the basin fills, did not reach shallower areas where paleoshorelines or erosional features would allow to better characterize and quantify the impact of past lake-level lowstands (Anselmetti et al., 2006). Nevertheless, collected evidence from Towuti clearly points to a close interplay between climate-induced lake-level changes and associated sedimentation rates with frequency and thickness of seismoturbidites (Figs. 8 and 9), an interference that needs to be taken into account when interpreting a seismic event catalogue based solely on the turbidite record.

6. Conclusion and perspectives

Correlation of sediment piston-core lithologies with seismic reflection data enabled us to establish a lithology-based high-resolution seismic stratigraphy of Lake Towuti. The particular morphology of the lake, with basins separated by tectonically-controlled bedrock ridges, induces a complex and heterogeneous sedimentation within the different basins, accentuated by their variation in depth.

Based on seismic reflection, lithological and petrophysical data, we established a detailed unit subclassification scheme for Lake Towuti's upper lacustrine sediment fill (Unit 1 in Russell et al. (2020b)). This scheme is based on the appearance of different and alternating lithotypes comprising green clays and red sideritic clays with more abundant turbidites and coinciding seismic reflection data with higher amplitudes in the red versus the green clays. Turbidites are particularly abundant with thicknesses reaching several decimetres in some of the basins during a last glacial/MIS 2 lake-level lowstand phase. Analysis of lithological characteristics, petrophysical parameters alongside seismic reflection data suggest that these turbidites predominantly originate from mass-transport processes triggered by seismic shaking. Differences in the abundance and thickness of turbidites between the different lake basins indicate varying susceptibilities of slopes to failure, primarily due to differences in slope angle and sedimentation rate.

Comparison of the seismological catalogue since the beginning of the 20th century with the Towuti turbidite record suggests an overall low sensitivity of Lake Towuti to record moderate earthquakes as a result of low sedimentation rates and reduced slope

charging in this tropical setting. Given the higher abundance of seismo-turbidites during the MIS 2 lowstand phase, we suggest a strong climatic influence on slope sensitivity to failure. Lake-level lowstands at Lake Towuti cause sediment remobilisation from the exposed shoreline and shelf onto the slope and into the basins' depocenters thereby increasing slope-charging rates and sensitivity to failure. This process is supported by overall higher background sedimentation rates in all of the lake basins during the lowstand phase when compared to the preceding and following highstand phases. The interplay of climate, sediment slope-charging, and mass-transport deposits at Lake Towuti may, while complicating the establishment of an accurate earthquake catalogue, serve as a valuable quantitative hydroclimate indicator. In the case of Lake Towuti, higher frequency turbidites indicates lake-level lowstand phases and coinciding drier regional climate conditions. Additional studies from other regional settings are required to fully exploit this relationship for paleoclimate reconstructions but the basin-scale results provided here appear promising.

Author contributions

NT and HV designed the study with input from SCF, JMR and FSA. NT and HV co-wrote the manuscript with input from all co-authors. JMR, NW and SB collected seismic data and JMR, HV, SYC and SB collected sediment piston cores from Lake Towuti. JMR and SB generated petrophysical datasets at the LacCore facilities.

Declaration of competing interest

The authors declare that they have no known competing financial interests or personal relationships that could have appeared to influence the work reported in this paper.

Data availability

Data will be made available on request.

Acknowledgements

This research was carried out with support from the German Research Foundation (DFG) and the Swiss National Science Foundation, Switzerland (SNSF) through grants awarded to H. Vogel (DFG: VO 1591/2–1; SNSF: 200020_188876 & 200021_153053) as well as through the U.S. National Science Foundation (NSF) through grants awarded to J.M. Russell. Foreign research permits for field work at Lake Towuti were kindly granted by the Ministry of Research, Education, and Higher Technology of Indonesia (RISTEK) permit number 02/TKPIPA/FRP/SM/II/2010. Logistical support was kindly provided by PT Vale Indonesia. We would like to acknowledge reviewers Katleen Wils and Maarten Van Daele who provided many helpful comments and suggestions which greatly helped to improve the manuscript.

Appendix A. Supplementary data

Supplementary data to this article can be found online at <https://doi.org/10.1016/j.quascirev.2023.108015>.

References

Adams, E.W., Schlager, W., Anselmetti, F.S., 2001. Morphology and curvature of delta slopes in Swiss lakes: lessons for the interpretation of clinofolds in seismic data. *Sedimentology* 48, 661–679. <https://doi.org/10.1046/j.1365-3091.2001.00389.x>.

Anselmetti, F.S., Ariztegui, D., De Batist, M., Catalina Gebhardt, A., Haberzettl, T., Niessen, F., Ohlendorf, C., Zolitschka, B., 2009. Environmental history of

southern Patagonia unravelled by the seismic stratigraphy of Laguna Potrok Aike. *Sedimentology* 56, 873–892. <https://doi.org/10.1111/j.1365-3091.2008.01002.x>.

Anselmetti, F.S., Ariztegui, D., Hodell, D.A., Hillesheim, M.B., Brenner, M., Gilli, A., McKenzie, J.A., Mueller, A.D., 2006. Late Quaternary climate-induced lake level variations in Lake Petén Itzá, Guatemala, inferred from seismic stratigraphic analysis. *Palaeogeogr. Palaeoclimatol. Palaeoecol.* 230, 52–69. <https://doi.org/10.1016/j.palaeo.2005.06.037>.

Ariztegui, D., Chondrogianni, C., Lami, A., Guilizzoni, P., Lafargue, E., 2001. Lacustrine organic matter and the Holocene paleoenvironmental record of Lake Albano (central Italy). *J. Paleolimnol.* 26, 283–292. <https://doi.org/10.1023/A:1017585808433>.

Avşar, U., Hubert-Ferrari, A., De Batist, M., Schmidt, S., Fagel, N., 2015. Sedimentary records of past earthquakes in boraboy lake during the last ca 600 years (north anatolian fault, Turkey). *Palaeogeogr. Palaeoclimatol. Palaeoecol.* 433, 1–9. <https://doi.org/10.1016/j.palaeo.2015.04.031>.

Avşar, U., Jönsson, S., Avşar, Ö., Schmidt, S., 2016. Earthquake-induced soft-sediment deformations and seismically amplified erosion rates recorded in varved sediments of Köyceğiz Lake (SW Turkey). *J. Geophys. Res. Solid Earth* 121, 4767–4779. <https://doi.org/10.1002/2016JB012820>.

Badhani, S., Cattaneo, A., Collico, S., Urgeles, R., Dennielou, B., Leroux, E., Colin, F., Garziglia, S., Rabineau, M., Droz, L., 2020. Integrated geophysical, sedimentological and geotechnical investigation of submarine landslides in the Gulf of Lions (Western Mediterranean). *Geol. Soc. Lond. Spec. Publ.* 500, 359–376. <https://doi.org/10.1144/SP500-2019-175>.

Ballance, P.F., Reading, H.G. (Eds.), 1980. *Sedimentation in Oblique-Slip Mobile Zones*, Special Publication of the International Association of Sedimentologists. Blackwell Scientific Publications, New York. Distributed in the U.S.A. by Halsted Press, Oxford [Oxfordshire]; Boston, Mass.

Bao, H., Ampuero, J.-P., Meng, L., Fielding, E.J., Liang, C., Milliner, C.W.D., Feng, T., Huang, H., 2019. Early and persistent supershear rupture of the 2018 magnitude 7.5 Palu earthquake. *Nat. Geosci.* 12, 200–205. <https://doi.org/10.1038/s41561-018-0297-z>.

Bartov, Y., Sagy, A., 2004. Late Pleistocene extension and strike-slip in the Dead Sea basin. *Geol. Mag.* 141, 565–572. <https://doi.org/10.1017/S001675680400963X>.

Bartov, Y., Stein, M., Enzel, Y., Agnon, A., Reches, Z., 2002. Lake levels and sequence stratigraphy of Lake Lisan, the late Pleistocene precursor of the Dead Sea. *Quat. Res.* 57, 9–21. <https://doi.org/10.1006/qres.2001.2284>.

Beck, C., 2009. Late Quaternary lacustrine paleo-seismic archives in north-western Alps: examples of earthquake-origin assessment of sedimentary disturbances. *Earth Sci. Rev.* 96, 327–344. <https://doi.org/10.1016/j.earscirev.2009.07.005>.

Belferman, M., Katsman, R., Agnon, A., 2018. Effect of large-scale surface water level fluctuations on earthquake recurrence interval under strike-slip faulting. *Tectonophysics* 744, 390–402. <https://doi.org/10.1016/j.tecto.2018.06.004>.

Bellier, O., Sebrier, M., Beaudouin, T., Villeneuve, M., Braucher, R., Bourles, D., Siame, L., Putranto, E., Pratomo, I., 2001. High slip rate for a low seismicity along the Palu-Koro active fault in central Sulawesi (Indonesia). *Terra. Nova* 13, 463–470. <https://doi.org/10.1046/j.1365-3121.2001.00382.x>.

Bellier, O., Sebrier, M., Seward, D., Beaudouin, T., Villeneuve, M., Putranto, E., 2006. Fission track and fault kinematics analyses for new insight into the Late Cenozoic tectonic regime changes in West-Central Sulawesi (Indonesia). *Tectonophysics* 413, 201–220. <https://doi.org/10.1016/j.tecto.2005.10.036>.

Biscontin, G., Pestana, J.M., Nadim, F., 2004. Seismic triggering of submarine slides in soft cohesive soil deposits. *Mar. Geol.* 203, 341–354. [https://doi.org/10.1016/S0025-3227\(03\)00314-1](https://doi.org/10.1016/S0025-3227(03)00314-1).

Blaauw, M., 2010. Methods and code for 'classical' age-modelling of radiocarbon sequences. *Quat. Geochronol.* 5, 512–518. <https://doi.org/10.1016/j.quageo.2010.01.002>.

Blumberg, S., Lamy, F., Arz, H.W., Ehtler, H.P., Wiedicke, M., Haug, G.H., Oncken, O., 2008. Turbiditic trench deposits at the South-Chilean active margin: a Pleistocene–Holocene record of climate and tectonics. *Earth Planet Sci. Lett.* 268, 526–539. <https://doi.org/10.1016/j.epsl.2008.02.007>.

Boncio, P., Amoroso, S., Galadini, F., Galderisi, A., Iezzi, G., Liberi, F., 2020. Earthquake-induced liquefaction features in a late Quaternary fine-grained lacustrine succession (Fucino Lake, Italy): implications for microzonation studies. *Eng. Geol.* 272, 105621. <https://doi.org/10.1016/j.enggeo.2020.105621>.

Bookman, R., Bartov, Y., Enzel, Y., Stein, M., 2006. Quaternary lake levels in the Dead Sea basin: two centuries of research. In: *New Frontiers in Dead Sea Paleoenvironmental Research*. Geological Society of America. [https://doi.org/10.1130/2006.2401\(10](https://doi.org/10.1130/2006.2401(10).

Brothers, D.S., Luttrell, K.M., Chaytor, J.D., 2013. Sea-level-induced seismicity and submarine landslide occurrence. *Geology* 41, 979–982. <https://doi.org/10.1130/G34410.1>.

Chapron, E., 1999. *Contrôles climatique et sismo-tectonique de la sédimentation lacustre dans l'avant pays alpin (Lac du Bourget) durant le quaternaire récent. (Alpes françaises) (Memoire H.S.)*. Université de Grenoble. Laboratoire de Géodynamique des Chaînes Alpines.

Chapron, E., Ariztegui, D., Mulsow, S., Villarosa, G., Pino, M., Outes, V., Juvigné, E., Crivelli, E., 2006. Impact of the 1960 major subduction earthquake in Northern Patagonia (Chile, Argentina). *Quat. Int.* 158, 58–71. <https://doi.org/10.1016/j.quaint.2006.05.017>.

Chapron, E., Simonneau, A., Ledoux, G., Arnaud, F., Lajeunesse, P., Albéric, P., 2016. French alpine foreland Holocene paleoseismicity revealed by coeval mass wasting deposits in glacial lakes. In: Lamarche, G., Mountjoy, J., Bull, S., Hubble, T., Krastel, S., Lane, E., Micallef, A., Moscardelli, L., Mueller, C., Pecher, I.,

- Woelz, S. (Eds.), *Submarine Mass Movements and Their Consequences, Advances in Natural and Technological Hazards Research*. Springer International Publishing, Cham, pp. 341–349. https://doi.org/10.1007/978-3-319-20979-1_34.
- Chassiot, L., Chapron, E., Di Giovanni, C., Lajeunesse, P., Tachikawa, K., Garcia, M., Bard, E., 2016. Historical seismicity of the Mont Dore volcanic province (Auvergne, France) unraveled by a regional lacustrine investigation: new insights about lake sensitivity to earthquakes. *Sediment. Geol.* 339, 134–150. <https://doi.org/10.1016/j.sedgeo.2016.04.007>.
- Closson, D., Abou Karaki, N., Hallot, F., 2010. Landslides along the Jordanian Dead Sea coast triggered by the lake level lowering. *Environ. Earth Sci.* 59, 1417–1430. <https://doi.org/10.1007/s12665-009-0128-z>.
- Collico, S., Arroyo, M., Urgeles, R., Gràcia, E., Devincenzi, M., Pérez, N., 2020. Probabilistic mapping of earthquake-induced submarine landslide susceptibility in the South-West Iberian margin. *Mar. Geol.* 429, 106296. <https://doi.org/10.1016/j.margeo.2020.106296>.
- Costa, K.M., Russell, J.M., Vogel, H., Bijaksana, S., 2015. Hydrological connectivity and mixing of Lake Towuti, Indonesia in response to paleoclimatic changes over the last 60,000 years. *Palaeogeogr. Palaeoclimatol.* 417, 467–475. <https://doi.org/10.1016/j.palaeo.2014.10.009>.
- Crowe, S.A., O'Neill, A.H., Katsev, S., Hehanussa, P., Haffner, G.D., Sundby, B., Mucci, A., Fowle, D.A., 2008. The biogeochemistry of tropical lakes: a case study from Lake Matano, Indonesia. *Limnol. Oceanogr.* 53, 319–331. <https://doi.org/10.4319/lo.2008.53.1.0319>.
- Daryono, M.R., Kumarawarman, B., Muslim, I.H., Triwujani, R., Permadi, R., Prihatmoko, S., Wibowo, S., Tutuko, G.H., 2021. Two earthquake events on the pampo segment of the Matano fault, Sulawesi. *IOP Conf. Ser. Earth Environ. Sci.* 873, 012053. <https://doi.org/10.1088/1755-1315/873/1/012053>.
- Daxer, C., Ortler, M., Fabbri, S.C., Hilbe, M., Hajdas, I., Dubois, N., Piechl, T., Hammerl, C., Strasser, M., Moernaut, J., 2022. High-resolution calibration of seismically-induced lacustrine deposits with historical earthquake data in the Eastern Alps (Carinthia, Austria). *Quat. Sci. Rev.* 284, 107497. <https://doi.org/10.1016/j.quascirev.2022.107497>.
- De Deckker, P., Tapper, N.J., van der Kaars, S., 2003. The status of the indo-pacific warm pool and adjacent land at the last glacial maximum. *Global Planet. Change* 35, 25–35. [https://doi.org/10.1016/S0921-8181\(02\)00089-9](https://doi.org/10.1016/S0921-8181(02)00089-9).
- Dente, E., Lensky, N.G., Morin, E., Enzel, Y., 2021. From straight to deeply incised meandering channels: slope impact on sinuosity of confined streams. *Earth Surf. Process. Landforms* 46, 1041–1054. <https://doi.org/10.1002/esp.5085>.
- Field, M.E., Gardner, J.V., Jennings, A.E., Edwards, B.D., 1982. Earthquake-induced sediment failures on a 0.25° slope, Klamath River delta, California. *Geology* 10, 542. [https://doi.org/10.1130/0091-7613\(1982\)10<542:ESFOAS>2.0.CO](https://doi.org/10.1130/0091-7613(1982)10<542:ESFOAS>2.0.CO).
- Gasparini, L., Marzocchi, A., Mazza, S., Miele, R., Meli, M., Najjar, H., Michetti, A.M., Polonia, A., 2020. Morphotectonics and late quaternary seismic stratigraphy of Lake Garda (northern Italy). *Geomorphology* 371, 107427. <https://doi.org/10.1016/j.geomorph.2020.107427>.
- Gastineau, R., de Sigoyer, J., Sabatier, P., Fabbri, S.C., Anselmetti, F.S., Develle, A.L., Şahin, M., Gündüz, S., Niessen, F., Gebhardt, A.C., 2021. Active subaqueous fault segments in Lake iznik along the middle strand of the North anatolian fault, NW Turkey. *Tectonics* 40, e2020TC006404. <https://doi.org/10.1029/2020TC006404>.
- Gilli, A., Anselmetti, F.S., Ariztegui, D., Beres, M., McKenzie, J.A., Markgraf, V., 2004. Seismic stratigraphy, buried beach ridges and contourite drifts: the Late Quaternary history of the closed Lago Cardiel basin, Argentina (49°S): seismic stratigraphy of Lago Cardiel, Argentina. *Sedimentology* 52, 1–23. <https://doi.org/10.1111/j.1365-3091.2004.00677.x>.
- Goldfinger, C., 2011. Submarine paleoseismology based on turbidite records. *Ann. Rev. Mar. Sci.* 3, 35–66. <https://doi.org/10.1146/annurev-marine-120709-142852>.
- Goldstein, S.L., Kiro, Y., Torfstein, A., Kitagawa, H., Tierney, J., Stein, M., 2020. Revised chronology of the ICDP Dead Sea deep drill core relates drier-wetter-drier climate cycles to insolation over the past 220 kyr. *Quat. Sci. Rev.* 244, 106460. <https://doi.org/10.1016/j.quascirev.2020.106460>.
- Gràcia, E., Vizcaino, A., Escutia, C., Asioli, A., Rodés, Á., Pallàs, R., Garcia-Orellana, J., Lebreiro, S., Goldfinger, C., 2010. Holocene earthquake record offshore Portugal (SW Iberia): testing turbidite paleoseismology in a slow-convergence margin. *Quat. Sci. Rev.* 29, 1156–1172. <https://doi.org/10.1016/j.quascirev.2010.01.010>.
- Guyard, H., Chapron, E., St-Onge, G., Anselmetti, F.S., Arnaud, F., Magand, O., Francus, P., Mélières, M.-A., 2007. High-altitude varve records of abrupt environmental changes and mining activity over the last 4000 years in the Western French Alps (Lake Bramant, Grandes Rousses Massif). *Quat. Sci. Rev.* 26, 2644–2660. <https://doi.org/10.1016/j.quascirev.2007.07.007>.
- Hage, S., Hubert-Ferrari, A., Lamair, L., Avşar, U., El Ouahabi, M., Van Daele, M., Boulvain, F., Ali Bahri, M., Seret, A., Plenevaux, A., 2017. Flow dynamics at the origin of thin clayey sand lacustrine turbidites: examples from Lake Hazar, Turkey. *Sedimentology* 64, 1929–1956. <https://doi.org/10.1111/sed.12380>.
- Hall, R., Wilson, M.E.J., 2000. Neogene sutures in eastern Indonesia. *J. Asian Earth Sci.* 18, 781–808. [https://doi.org/10.1016/S1367-9120\(00\)00040-7](https://doi.org/10.1016/S1367-9120(00)00040-7).
- Hamilton, R., Stevenson, J., Li, B., Bijaksana, S., 2019. A 16,000-year record of climate, vegetation and fire from Wallacean lowland tropical forests. *Quat. Sci. Rev.* 224, 105929. <https://doi.org/10.1016/j.quascirev.2019.105929>.
- Hamilton, W.B., 1972. Tectonics of the Indonesian Region (Report No. 72–1978), Open-File Report. <https://doi.org/10.3133/ofr721978>.
- Hansen, L., Waldmann, N., Storms, J.E.A., Eilertsen, R.S., Ariztegui, D., Chapron, E., Nesje, A., 2016. Morphological signatures of mass wasting and delta processes in a fjord-lake system: insights from Lovatnet, western Norway. *Nor. J. Geol.* <https://doi.org/10.17850/njg96-3-02>.
- Haq, B.U., 1998. Natural gas hydrates: searching for the long-term climatic and slope-stability records. *Geol. Soc. Lond. Spec. Publ.* 137, 303–318. <https://doi.org/10.1144/GSL.SP.1998.137.01.24>.
- Hasberg, A.K.M., Bijaksana, S., Held, P., Just, J., Melles, M., Morlock, M.A., Opitz, S., Russell, J.M., Vogel, H., Wennrich, V., 2019. Modern sedimentation processes in Lake Towuti, Indonesia, revealed by the composition of surface sediments. *Sedimentology* 66, 675–698. <https://doi.org/10.1111/sed.12503>.
- Howarth, J.D., Fitzsimons, S.J., Norris, R.J., Jacobsen, G.E., 2014. Lake sediments record high intensity shaking that provides insight into the location and rupture length of large earthquakes on the Alpine Fault, New Zealand. *Earth Planet. Sci. Lett.* 403, 340–351. <https://doi.org/10.1016/j.epsl.2014.07.008>.
- Howarth, J.D., Orpin, A.R., Kaneko, Y., Strachan, L.J., Nodder, S.D., Mountjoy, J.J., Barnes, P.M., Bostock, H.C., Holden, C., Jones, K., Çağatay, M.N., 2021. Calibrating the marine turbidite palaeoseismometer using the 2016 Kaikōura earthquake. *Nat. Geosci.* 14, 161–167. <https://doi.org/10.1038/s41561-021-00692-6>.
- Hubert-Ferrari, A., Lamair, L., Hage, S., Schmidt, S., Çağatay, M.N., Avşar, U., 2020. A 3800 yr paleoseismic record (Lake Hazar sediments, eastern Turkey): implications for the East Anatolian Fault seismic cycle. *Earth Planet. Sci. Lett.* 538, 116152. <https://doi.org/10.1016/j.epsl.2020.116152>.
- Hutchinson, D.R., Golmshtok, A.J., Zonenshain, L.P., Moore, T.C., Scholz, C.A., Klitgord, K.D., 1992. Depositional and Tectonic Framework of the Rift Basins of Lake Baikal from Multichannel Seismic Data 5.
- Inouchi, Y., Kinugasa, Y., Kumon, F., Nakano, S., Yasumatsu, S., Shiki, T., 1996. Turbidites as records of intense palaeoearthquakes in Lake Biwa, Japan. *Sediment. Geol.* 104, 117–125. [https://doi.org/10.1016/0037-0738\(95\)00124-7](https://doi.org/10.1016/0037-0738(95)00124-7).
- Irsyam, M., Cummins, P.R., Asrurifak, M., Faizal, L., Natawidjaja, D.H., Widiyantoro, S., Meilano, I., Triyoso, W., Rudiyanto, A., Hidayati, S., Ridwan, M., Hanifa, N.R., Syahbana, A.J., 2020. Development of the 2017 national seismic hazard maps of Indonesia. *Earthq. Spectra* 36, 112–136. <https://doi.org/10.1177/875293020951206>.
- Kadariusman, A., Miyashita, S., Maruyama, S., Parkinson, C.D., Ishikawa, A., 2004. Petrology, geochemistry and paleogeographic reconstruction of the East Sulawesi ophiolite, Indonesia. *Tectonophysics* 392, 55–83. <https://doi.org/10.1016/j.tecto.2004.04.008>.
- Kempf, J., Moernaut, J., Van Daele, M., Pino, M., Urrutia, R., De Batist, M., 2020. Paleotsunami record of the past 4300 years in the complex coastal lake system of Lake Cucao, Chiloe Island, south central Chile. *Sediment. Geol.* 401, 105644. <https://doi.org/10.1016/j.sedgeo.2020.105644>.
- Konecky, B., Russell, J., Bijaksana, S., 2016. Glacial aridity in central Indonesia coeval with intensified monsoon circulation. *Earth Planet. Sci. Lett.* 437, 15–24. <https://doi.org/10.1016/j.epsl.2015.12.037>.
- Krause, C.E., Gagan, M.K., Dunbar, G.B., Hantoro, W.S., Hellstrom, J.C., Cheng, H., Edwards, R.L., Suwargadi, B.W., Abram, N.J., Rifai, H., 2019. Spatio-temporal evolution of Australasian monsoon hydroclimate over the last 40,000 years. *Earth Planet. Sci. Lett.* 513, 103–112. <https://doi.org/10.1016/j.epsl.2019.01.045>.
- Kremer, K., Corella, J.P., Adatte, T., Garnier, E., Zenhäusern, gregor, Girardclos, S., 2015. Origin of turbidites in deep lake Geneva (France–Switzerland) in the last 1500 years. *J. Sediment. Res.* 85, 1455–1465. <https://doi.org/10.2110/jsr.2015.92>.
- Kremer, K., Wirth, S.B., Reusch, A., Fäh, D., Bellwald, B., Anselmetti, F.S., Girardclos, S., Strasser, M., 2017. Lake-sediment based paleoseismology: limitations and perspectives from the Swiss Alps. *Quat. Sci. Rev.* 168, 1–18. <https://doi.org/10.1016/j.quascirev.2017.04.026>.
- Lafuente, P., Arlegui, L.E., Liesa, C.L., Pueyo, Ó., Simón, J.L., 2014. Spatial and temporal variation of palaeoseismic activity at an intraplate, historically quiescent structure: the Conclud fault (Iberian Chain, Spain). *Tectonophysics* 632, 167–187. <https://doi.org/10.1016/j.tecto.2014.06.012>.
- Lauterbach, S., Chapron, E., Brauer, A., Hüls, M., Gilli, A., Arnaud, F., Piccin, A., Nomade, J., Desmet, M., von Grafenstein, U., Participants, D., 2012. A sedimentary record of Holocene surface runoff events and earthquake activity from Lake Iseo (Southern Alps, Italy). *Holocene* 22, 749–760. <https://doi.org/10.1177/0959683611430340>.
- Lee, H.J., Chough, S.K., Yoon, S.H., 1996. Slope-stability change from late Pleistocene to Holocene in the ulleung basin, east sea (Japan sea). *Sediment. Geol.* 104, 39–51. [https://doi.org/10.1016/0037-0738\(95\)00119-0](https://doi.org/10.1016/0037-0738(95)00119-0).
- Leithold, E.L., Wegmann, K.W., Bohnenstiehl, D.R., Joyner, C.N., Pollen, A.F., 2019. Repeated megaturbidite deposition in Lake Crescent, Washington, USA, triggered by Holocene ruptures of the Lake Creek-boundary Creek fault system. *Geol. Soc. Am. Bull.* 131.
- Leithold, E.L., Wegmann, K.W., Bohnenstiehl, D.R., Smith, S.G., Noren, A., O'Grady, R., 2018. Slope failures within and upstream of Lake Quinault, Washington, as uneven responses to Holocene earthquakes along the Cascadia subduction zone. *Quat. Res.* 89, 178–200. <https://doi.org/10.1017/qua.2017.96>.
- Leonard, M., 2015. Consistent MMI area estimation for Australian earthquakes. In: *Proceedings of the Tenth Pacific Conference on Earthquake Engineering Building an Earthquake-Resilient Pacific*, p. 9. Presented at the PCCE 2015, Geoscience Australia, Sydney, Australia.
- Leynaud, D., Sultan, N., Mienert, J., 2007. The role of sedimentation rate and permeability in the slope stability of the formerly glaciated Norwegian continental margin: the Storegga slide model. *Landslides* 4, 297–309. <https://doi.org/10.1007/s10346-007-0086-z>.
- Lu, Y., Moernaut, J., Bookman, R., Waldmann, N., Wetzler, N., Agnon, A., Marco, S., Alsop, G.I., Strasser, M., Hubert-Ferrari, A., 2021a. A new approach to constrain the seismic origin for prehistoric turbidites as applied to the Dead Sea basin. *Geophys. Res. Lett.* 48. <https://doi.org/10.1029/2020GL090947>.

- Lu, Y., Moernaut, J., Waldmann, N., Bookman, R., Alsop, G.I., Hubert-Ferrari, A., Strasser, M., Agnon, A., Marco, S., 2021b. Orbital- and millennial-scale changes in lake-levels facilitate earthquake-triggered mass failures in the Dead Sea Basin. *Geophys. Res. Lett.* e2021GL093391 24. <https://doi.org/10.1029/2021GL093391>.
- Ma, T., Tarasov, P.E., Huang, K., Leipe, C., Man, M., Zheng, Z., 2022. Intensified climate drying and cooling during the last glacial culmination (20.8–17.5 cal ka BP) in the south-eastern Asian monsoon domain inferred from a high-resolution pollen record. *Quat. Sci. Rev.* 278, 107371. <https://doi.org/10.1016/j.quascirev.2022.107371>.
- Maitituerdi, A., Van Daele, M., Verschuren, D., De Batist, M., Waldmann, N., 2022. Depositional history of Lake Chala (Mt. Kilimanjaro, equatorial East Africa) from high-resolution seismic stratigraphy. *J. Afr. Earth Sci.* 104499 <https://doi.org/10.1016/j.jafrearsci.2022.104499>.
- McHugh, C.M.G., Damuth, J.E., Mountain, G.S., 2002. Cenozoic mass-transport facies and their correlation with relative sea-level change, New Jersey continental margin. *Mar. Geol.* 184, 295–334. [https://doi.org/10.1016/S0025-3227\(01\)00240-7](https://doi.org/10.1016/S0025-3227(01)00240-7).
- Melles, M., Brigham-Grette, J., Minyuk, P.S., Nowaczyk, N.R., Wennrich, V., DeConto, R.M., Anderson, P.M., Andreev, A.A., Coletti, A., Cook, T.L., Haltia-Hovi, E., Kukkonen, M., Lozhkin, A.V., Rosén, P., Tarasov, P., Vogel, H., Wagner, B., 2012. 2.8 million years of arctic climate change from Lake El'gygytgyn, NE Russia. *Science* 337, 315–320. <https://doi.org/10.1126/science.1222135>.
- Moernaut, J., 2020. Time-dependent recurrence of strong earthquake shaking near plate boundaries: a lake sediment perspective. *Earth Sci. Rev.* 210, 103344. <https://doi.org/10.1016/j.earscirev.2020.103344>.
- Moernaut, J., Daele, M.V., Fontijn, K., Heirman, K., Kempf, P., Pino, M., Valdebenito, G., Urrutia, R., Strasser, M., Batist, M.D., 2018. Larger earthquakes recur more periodically: new insights in the megathrust earthquake cycle from lacustrine turbidite records in south-central Chile. *Earth Planet Sci. Lett.* 481, 9–19. <https://doi.org/10.1016/j.epsl.2017.10.016>.
- Moernaut, J., Daele, M.V., Heirman, K., Fontijn, K., Strasser, M., Pino, M., Urrutia, R., De Batist, M., 2014. Lacustrine turbidites as a tool for quantitative earthquake reconstruction: new evidence for a variable rupture mode in south central Chile. *J. Geophys. Res. Solid Earth* 119, 1607–1633. <https://doi.org/10.1002/2013JB010738>.
- Moernaut, J., De Batist, M., 2011. Frontal emplacement and mobility of sublacustrine landslides: results from morphometric and seismostratigraphic analysis. *Mar. Geol.* 285, 29–45. <https://doi.org/10.1016/j.margeo.2011.05.001>.
- Moernaut, J., De Batist, M., Charlet, F., Heirman, K., Chapron, E., Pino, M., Brümmer, R., Urrutia, R., 2007. Giant earthquakes in south-Central Chile revealed by Holocene mass-wasting events in Lake Puyehue. *Sediment. Geol.* 195, 239–256. <https://doi.org/10.1016/j.sedgeo.2006.08.005>.
- Moernaut, J., Verschuren, D., Charlet, F., Kristen, I., Fagot, M., De Batist, M., 2010. The seismic-stratigraphic record of lake-level fluctuations in Lake Challa: hydrological stability and change in equatorial East Africa over the last 140kyr. *Earth Planet Sci. Lett.* 290, 214–223. <https://doi.org/10.1016/j.epsl.2009.12.023>.
- Molenaar, A., Moernaut, J., Wiemer, G., Dubois, N., Strasser, M., 2019. Earthquake impact on active margins: tracing surficial remobilization and seismic strengthening in a slope sedimentary sequence. *Geophys. Res. Lett.* 46, 6015–6023. <https://doi.org/10.1029/2019GL082350>.
- Molenaar, A., Van Daele, M., Vandorpe, T., Degenhart, G., De Batist, M., Urrutia, R., Pino, M., Strasser, M., Moernaut, J., 2021. What controls the remobilization and deformation of surficial sediment by seismic shaking? Linking lacustrine slope stratigraphy to great earthquakes in South–Central Chile. *Sedimentology* 68, 2365–2396. <https://doi.org/10.1111/sed.12856>.
- Morlock, M., 2018. *Depositional Modes and Post-depositional Mineral Formation in a Pleistocene Sediment Record from Lake Towuti, Indonesia* (PhD Thesis). Universität Bern, Bern.
- Morlock, M.A., Vogel, H., Nigg, V., Ordoñez, L., Hasberg, A.K.M., Melles, M., Russell, J.M., Bijaksana, S., 2019. Climatic and tectonic controls on source-to-sink processes in the tropical, ultramafic catchment of Lake Towuti, Indonesia. *J. Paleolimnol.* 61, 279–295. <https://doi.org/10.1007/s10933-018-0059-3>.
- Morlock, M.A., Vogel, H., Russell, J.M., Anselmetti, F.S., Bijaksana, S., 2021. Quaternary environmental changes in tropical Lake Towuti, Indonesia, inferred from end-member modelling of X-ray fluorescence core-scanning data. *J. Quat. Sci.* 36, 1040–1051. <https://doi.org/10.1002/jqs.3338>.
- Natawidjaja, D.H., Daryono, M.R., Prasetya, G., Udrek, Liu, P.L.-F., Hananto, N.D., Kongko, W., Triyoso, W., Puji, A.R., Meilano, I., Gunawan, E., Supendi, P., Pamumpuni, A., Irsyam, M., Faizal, L., Hidayati, S., Sapiie, B., Kusuma, M.A., Tawil, S., 2020. The 2018 Mw7.5 Palu 'supershear' earthquake ruptures geological fault's multi-segment separated by large bends: results from integrating field measurements, LiDAR, swath bathymetry, and seismic-reflection data. *Geophys. J. Int.* ggaa498. <https://doi.org/10.1093/gji/ggaa498>.
- Nayak, K., Lin, A.T.-S., Huang, K.-F., Liu, Z., Babonneau, N., Ratzov, G., Pillutla, R.K., Das, P., Hsu, S.-K., 2021. Clay-mineral distribution in recent deep-sea sediments around Taiwan: implications for sediment dispersal processes. *Tectonophysics* 814, 228974. <https://doi.org/10.1016/j.tecto.2021.228974>.
- Neves, M.C., Roque, C., Luttrell, K.M., Vázquez, J.T., Alonso, B., 2016. Impact of sea-level rise on earthquake and landslide triggering offshore the Alentejo margin (SW Iberia). *Geo Mar. Lett.* 36, 415–424. <https://doi.org/10.1007/s00367-016-0459-1>.
- Omira, R., Dogan, G.G., Hidayat, R., Husrin, S., Prasetya, G., Annunziato, A., Proietti, C., Probst, P., Paparo, M.A., Wronna, M., Zaytsev, A., Pronin, P., Giniyatullin, A., Putra, P.S., Hartanto, D., Ginanjar, G., Kongko, W., Pelinovsky, E., Yalciner, A.C., 2019. The september 28th, 2018, tsunami in palu-sulawesi, Indonesia: a post-event field survey. *Pure Appl. Geophys.* 176, 1379–1395. <https://doi.org/10.1007/s00024-019-02145-z>.
- Oswald, P., Moernaut, J., Fabbri, S.C., De Batist, M., Hajdas, I., Ortner, H., Titzler, S., Strasser, M., 2021. Combined on-fault and off-fault paleoseismic evidence in the postglacial infill of the inner-alpine lake achensee (Austria, eastern Alps). *Front. Earth Sci.* 9, 670952. <https://doi.org/10.3389/feart.2021.670952>.
- Owen, M., Day, S., Maslin, M., 2007. Late Pleistocene submarine mass movements: occurrence and causes. *Quat. Sci. Rev.* 26, 958–978. <https://doi.org/10.1016/j.quascirev.2006.12.011>.
- Partin, J.W., Cobb, K.M., Adkins, J.F., Clark, B., Fernandez, D.P., 2007. Millennial-scale trends in west Pacific warm pool hydrology since the Last Glacial Maximum. *Nature* 449, 452–455. <https://doi.org/10.1038/nature06164>.
- Pohl, F., Eggenhuisen, J.T., Cartigny, M.J.B., Tilston, M.C., de Leeuw, J., Hermidas, N., 2020. The influence of a slope break on turbidite deposits: an experimental investigation. *Mar. Geol.* 424, 106160. <https://doi.org/10.1016/j.margeo.2020.106160>.
- Praet, N., Moernaut, J., Van Daele, M., Boes, E., Haeussler, P.J., Strupler, M., Schmidt, S., Loso, M.G., De Batist, M., 2017. Paleoseismic potential of sublacustrine landslide records in a high-seismicity setting (south-central Alaska). *Mar. Geol.* 384, 103–119. <https://doi.org/10.1016/j.margeo.2016.05.004>.
- Praet, N., Van Daele, M., Collart, T., Moernaut, J., Vandekerckhove, E., Kempf, P., Haeussler, P.J., De Batist, M., 2020. Turbidite stratigraphy in proglacial lakes: deciphering trigger mechanisms using a statistical approach. *Sedimentology* 67, 2332–2359. <https://doi.org/10.1111/sed.12703>.
- Ratzov, G., Cattaneo, A., Babonneau, N., Déverchère, J., Yelles, K., Bracene, R., Courboux, F., 2015. Holocene turbidites record earthquake supercycles at a slow-rate plate boundary. *Geology* 43, 331–334. <https://doi.org/10.1130/G36170.1>.
- Reeves, J.M., Bostock, H.C., Ayliffe, L.K., Barrows, T.T., De Deckker, P., Devriendt, L.S., Dunbar, G.B., Drysdale, R.N., Fitzsimmons, K.E., Gagan, M.K., Griffiths, M.L., Haberle, S.G., Jansen, J.D., Krause, C., Lewis, S., McGregor, H.V., Mooney, S.D., Moss, P., Nanson, G.C., Purcell, A., van der Kaars, S., 2013. Palaeoenvironmental change in tropical Australasia over the last 30,000 years – a synthesis by the OZ-INTIMATE group. *Quat. Sci. Rev.* 74, 97–114. <https://doi.org/10.1016/j.quascirev.2012.11.027>.
- Reimer, P.J., Austin, W.E.N., Bard, E., Bayliss, A., Blackwell, P.G., Bronk Ramsey, C., Butzin, M., Cheng, H., Edwards, R.L., Friedrich, M., Grootes, P.M., Guilderson, T.P., Hajdas, I., Heaton, T.J., Hogg, A.G., Hughen, K.A., Kromer, B., Manning, S.W., Muscheler, R., Palmer, J.G., Pearson, C., van der Plicht, J., Reimer, R.W., Richards, D.A., Scott, E.M., Southon, J.R., Turney, C.S.M., Wacker, L., Adolphi, F., Büntgen, U., Capano, M., Fahrni, S.M., Fogtmann-Schulz, A., Friedrich, R., Köhler, P., Kudsk, S., Miyake, F., Olsen, J., Reinig, F., Sakamoto, M., Sookdeo, A., Talamo, S., 2020. The IntCal20 northern hemisphere radiocarbon age calibration curve (0–55 cal kBP). *Radiocarbon* 62, 725–757. <https://doi.org/10.1017/RDC.2020.41>.
- Russell, J.M., Barker, P., Cohen, A., Ivory, S., Kimirei, I., Lane, C., Leng, M., Maganza, N., McGlue, M., Msaky, E., Noren, A., Park Boush, L., Salzburger, W., Scholz, C., Tiedemann, R., Nuru, S., 2020a. The Lake Tanganyika Scientific Drilling Project (TSDP) Consortium, 2020a. ICDP workshop on the Lake Tanganyika Scientific Drilling Project: a late Miocene–present record of climate, rifting, and ecosystem evolution from the world's oldest tropical lake. *Sci. Drill.* 27, 53–60. <https://doi.org/10.5194/sd-27-53-2020>.
- Russell, J.M., Bijaksana, S., 2012. The Towuti drilling Project: paleoenvironments, biological evolution, and geomicrobiology of a tropical Pacific lake. *Sci. Drill.* 14, 68–71. <https://doi.org/10.2204/ioldp.sd.14.11.2012>.
- Russell, J.M., Bijaksana, S., Vogel, H., Melles, M., Kallmeyer, J., Ariztegui, D., Crowe, S., Fajar, S., Hafidz, A., Haffner, D., Hasberg, A., Ivory, S., Kelly, C., King, J., Kirana, K., Morlock, M., Noren, A., O'Grady, R., Ordoñez, L., Stevenson, J., von Rintelen, T., Vuillemin, A., Watkinson, I., Wattrus, N., Wicaksono, S., Wonik, T., Bauer, K., Deino, A., Friese, A., Henny, C., Imran, Marwoto, R., Ngkoimani, L.O., Nomosatryo, S., Safiuddin, L.O., Simister, R., Tamuntuan, G., 2016. The Towuti Drilling Project: paleoenvironments, biological evolution, and geomicrobiology of a tropical Pacific lake. *Sci. Drill.* 21, 29–40. <https://doi.org/10.5194/sd-21-29-2016>.
- Russell, J.M., Vogel, H., Bijaksana, S., Melles, M., Deino, A., Hafidz, A., Haffner, D., Hasberg, A.K.M., Morlock, M., von Rintelen, T., Sheppard, R., Stelbrink, B., Stevenson, J., 2020b. The late quaternary tectonic, biogeochemical, and environmental evolution of ferruginous Lake Towuti, Indonesia. *Palaeogeogr. Palaeoclimatol. Palaeoecol.* 109905 <https://doi.org/10.1016/j.palaeo.2020.109905>.
- Russell, J.M., Vogel, H., Konecky, B.L., Bijaksana, S., Huang, Y., Melles, M., Wattrus, N., Costa, K., King, J.W., 2014. Glacial forcing of central Indonesian hydroclimate since 60,000 y B.P. *Proc. Natl. Acad. Sci. USA* 111, 5100–5105. <https://doi.org/10.1073/pnas.1402373111>.
- Sabatier, P., Moernaut, J., Bertrand, S., Van Daele, M., Kremer, K., Chaumillon, E., Arnaud, F., 2022. A review of event deposits in Lake sediments. *Quaternary* 5, 34. <https://doi.org/10.3390/quat5030034>.
- Sammartini, M., Moernaut, J., Kopf, A., Stegmann, S., Fabbri, S.C., Anselmetti, F.S., Strasser, M., 2021. Propagation of frontally confined subaqueous landslides: insights from combining geophysical, sedimentological, and geotechnical analysis. *Sediment. Geol.* 416, 105877. <https://doi.org/10.1016/j.sedgeo.2021.105877>.
- Schnellmann, M., Anselmetti, F.S., Giardini, D., McKENZIE, J.A., 2005. Mass

- movement-induced fold-and-thrust belt structures in unconsolidated sediments in Lake Lucerne (Switzerland): mass movement-induced deformation structures. *Sedimentology* 52, 271–289. <https://doi.org/10.1111/j.1365-3091.2004.00694.x>.
- Schnellmann, M., Anselmetti, F.S., Giardini, D., McKenzie, J.A., Ward, S.N., 2002. Prehistoric earthquake history revealed by lacustrine slump deposits. *Geology* 30, 1131. [https://doi.org/10.1130/0091-7613\(2002\)030<1131:PEHRBL>2.0.CO](https://doi.org/10.1130/0091-7613(2002)030<1131:PEHRBL>2.0.CO).
- Schwestermann, T., Huang, J., Konzett, J., Kioka, A., Wefer, G., Ikehara, K., Moernaut, J., Eglinton, T.I., Strasser, M., 2020. Multivariate statistical and multiproxy constraints on earthquake-triggered sediment remobilization processes in the Central Japan trench. *G-cubed* 21. <https://doi.org/10.1029/2019GC008861>.
- Shanahan, T.M., Overpeck, J.T., Wheeler, C.W., Beck, J.W., Pigati, J.S., Talbot, M.R., Scholz, C.A., Peck, J., King, J.W., 2006. Paleoclimatic variations in west Africa from a record of late Pleistocene and Holocene lake level stands of Lake Bosumtwi, Ghana. *Palaeogeogr. Palaeoclimatol. Palaeoecol.* 242, 287–302. <https://doi.org/10.1016/j.palaeo.2006.06.007>.
- Shiki, T., Kumon, F., Inouchi, Y., Kontani, Y., Sakamoto, T., Tateishi, M., Matsubara, H., Fukuyama, K., 2000. Sedimentary features of the seismo-turbidites, lake biwa, Japan. *Sediment. Geol.* 135, 37–50. [https://doi.org/10.1016/S0037-0738\(00\)00061-0](https://doi.org/10.1016/S0037-0738(00)00061-0).
- Shinohara, H., Yoshikawa, S., Miyabuchi, Y., 2015. Degassing activity of a volcanic crater lake: volcanic plume measurements at the yudamari crater lake, aso volcano, Japan. In: Rouwet, D., Christenson, B., Tassi, F., Vandemeulebrouck, J. (Eds.), *Volcanic Lakes*. Springer Berlin Heidelberg, Berlin, Heidelberg, pp. 201–217. https://doi.org/10.1007/978-3-642-36833-2_8.
- Silver, E.A., McCaffrey, R., Smith, R.B., 1983. Collision, rotation, and the initiation of subduction in the evolution of Sulawesi, Indonesia. *J. Geophys. Res. Solid Earth* 88, 9407–9418. <https://doi.org/10.1029/JB088iB11p09407>.
- Socquet, A., Simons, W., Vigny, C., McCaffrey, R., Subarya, C., Sarsito, D., Ambrosius, B., Spakman, W., 2006. Microblock rotations and fault coupling in SE Asia triple junction (Sulawesi, Indonesia) from GPS and earthquake slip vector data. *J. Geophys. Res.* 111, B08409. <https://doi.org/10.1029/2005JB003963>.
- Stevens, C., McCaffrey, R., Bock, Y., Genrich, J., Endang, Subarya, C., Puntodewo, S.S.O., Fauzi, Vigny, C., 1999. Rapid rotations about a vertical axis in a collisional setting revealed by the Palu Fault, Sulawesi, Indonesia. *Geophys. Res. Lett.* 26, 2677–2680. <https://doi.org/10.1029/1999GL008344>.
- St-Onge, G., Mulder, T., Piper, D.J.W., Hillaire-Marcel, C., Stoner, J.S., 2004. Earthquake and flood-induced turbidites in the saguenay fjord (Québec): a Holocene paleoseismicity record. *Quat. Sci. Rev.* 23, 283–294. <https://doi.org/10.1016/j.quascirev.2003.03.001>.
- Strasser, M., Berberich, T., Fabbri, S., Hilbe, M., Huang, J.-S., Lauterbach, S., Ortler, M., Rechsreiter, H., Brauer, A., Anselmetti, F., Kowarik, K., 2020. Geomorphology and event-stratigraphy of recent mass-movement processes in Lake Hallstatt (UNESCO world heritage Cultural landscape, Austria). *Geol. Soc. Lond. Spec. Publ.* 500, 405–426. <https://doi.org/10.1144/SP500-2019-178>.
- Strasser, M., Hilbe, M., Anselmetti, F.S., 2011. Mapping basin-wide subaquatic slope failure susceptibility as a tool to assess regional seismic and tsunami hazards. *Mar. Geophys. Res.* 32, 331–347. <https://doi.org/10.1007/s11001-010-9100-2>.
- Strasser, M., Monecke, K., Schnellmann, M., Anselmetti, F.S., 2013. Lake sediments as natural seismographs: a compiled record of Late Quaternary earthquakes in Central Switzerland and its implication for Alpine deformation. *Sedimentology* 60, 319–341. <https://doi.org/10.1111/sed.12003>.
- Strasser, M., Stegmann, S., Bussmann, F., Anselmetti, F.S., Rick, B., Kopf, A., 2007. Quantifying subaqueous slope stability during seismic shaking: lake Lucerne as model for ocean margins. *Mar. Geol.* 240, 77–97. <https://doi.org/10.1016/j.margeo.2007.02.016>.
- Strupler, M., Hilbe, M., Anselmetti, F.S., Kopf, A.J., Fleischmann, T., Strasser, M., 2017. Probabilistic stability evaluation and seismic triggering scenarios of submerged slopes in Lake Zurich (Switzerland). *Geo Mar. Lett.* 37, 241–258. <https://doi.org/10.1007/s00367-017-0492-8>.
- Sturm, M., Matter, A., 1978. Turbidites and varves in Lake brienz (Switzerland): deposition of clastic detritus by density currents. In: *Modern and Ancient Lake Sediments*. John Wiley & Sons, Ltd, pp. 147–168. <https://doi.org/10.1002/9781444303698.ch8>.
- Sultan, N., Cochonat, P., Canals, M., Cattaneo, A., Dennielou, B., Hafliadason, H., Laberg, J.S., Long, D., Mienert, J., Trincardi, F., Urgeles, R., Vorren, T.O., Wilson, C., 2004. Triggering mechanisms of slope instability processes and sediment failures on continental margins: a geotechnical approach. *Mar. Geol.* 213, 291–321. <https://doi.org/10.1016/j.margeo.2004.10.011>.
- Talling, P.J., 2021. Fidelity of turbidites as earthquake records. *Nat. Geosci.* 14, 113–116. <https://doi.org/10.1038/s41561-021-00707-2>.
- Tamuntuan, G., Bijaksana, S., King, J., Russell, J., Fauzi, U., Maryunani, K., Atifa, N., Safiuddin, L.O., 2015. Variation of magnetic properties in sediments from Lake Towuti, Indonesia, and its paleoclimatic significance. *Palaeogeogr. Palaeoclimatol. Palaeoecol.* 420, 163–172. <https://doi.org/10.1016/j.palaeo.2014.12.008>.
- Tauhid, Y.I., Arifian, J., 2000. *Pengamatan Jangka Panjang Kondisi Danau Towuti*. J. Sains Teknol. Modif. Cuaca 1, pp. 93–100.
- ten Brink, U.S., Andrews, B.D., Miller, N.C., 2016. Seismicity and sedimentation rate effects on submarine slope stability. *Geology* 44, 563–566. <https://doi.org/10.1130/G37866.1>.
- Tohari, A., Dani Wardhana, D., Hanif, M., Koizumi, K., 2021. Understanding of sub-surface conditions controlling flow liquefaction occurrence during the 2018 Palu earthquake based on resistivity profiles. *E3S Web Conf.* 331, 03002. <https://doi.org/10.1051/e3sconf/202133103002>.
- Urbaub, M., Talling, P.J., Zervos, A., Masson, D., 2015. What causes large submarine landslides on low gradient (<2°) continental slopes with slow (~0.15 m/kyr) sediment accumulation?: large submarine landslides on low gradients. *J. Geophys. Res. Solid Earth* 120, 6722–6739. <https://doi.org/10.1002/2015JB012347>.
- Vaillant, J.J., Haffner, G.D., Cristescu, M.E., 2011. The ancient lakes of Indonesia: towards integrated research on speciation. *Integr. Comp. Biol.* 51, 634–643. <https://doi.org/10.1093/icb/icr101>.
- Van Daele, M., Moernaut, J., Doom, L., Boes, E., Fontijn, K., Heirman, K., Vandoorne, W., Hebbeln, D., Pino, M., Urrutia, R., Brümmer, R., De Batist, M., 2015. A comparison of the sedimentary records of the 1960 and 2010 great Chilean earthquakes in 17 lakes: implications for quantitative lacustrine palaeoseismology. *Sedimentology* 62, 1466–1496. <https://doi.org/10.1111/sed.12193>.
- Vandekerckhove, E., Van Daele, M., Praet, N., Cnudde, V., Haeussler, P.J., De Batist, M., 2020. Flood-triggered versus earthquake-triggered turbidites: a sedimentological study in clastic lake sediments (Eklutna Lake, Alaska). *Sedimentology* 67, 364–389. <https://doi.org/10.1111/sed.12646>.
- Vanneste, K., Wils, K., Van Daele, M., 2018. Probabilistic evaluation of fault sources based on paleoseismic evidence from mass-transport deposits: the example of aysén fjord, Chile. *J. Geophys. Res. Solid Earth* 123, 9842–9865. <https://doi.org/10.1029/2018JB016289>.
- Villeneuve, M., Gunawan, W., Cornée, J.-J., Vidal, O., 2002. Geology of the central Sulawesi belt (eastern Indonesia): constraints for geodynamic models. *Int. J. Earth Sci.* 91, 524–537. <https://doi.org/10.1007/s005310100228>.
- Vogel, H., Russell, J.M., Cahyarini, S.Y., Bijaksana, S., Wattrus, N., Rethemeyer, J., Melles, M., 2015. Depositional modes and lake-level variability at Lake Towuti, Indonesia, during the past ~29 kyr BP. *J. Paleolimnol.* 54, 359–377. <https://doi.org/10.1007/s10933-015-9857-z>.
- Völker, D., Geersen, J., Behrmann, J.H., Weinrebe, W.R., 2012. Submarine mass wasting off southern Central Chile: distribution and possible mechanisms of slope failure at an active continental margin. In: Yamada, Y., Kawamura, K., Ikehara, K., Ogawa, Y., Urgeles, R., Mosher, D., Chaytor, J., Strasser, M. (Eds.), *Submarine Mass Movements and Their Consequences*. Springer Netherlands, Dordrecht, pp. 379–389. https://doi.org/10.1007/978-94-007-2162-3_34.
- Vuillemin, A., Wirth, R., Kemnitz, H., Schleicher, A.M., Friebe, A., Bauer, K.W., Simister, R., Nomosatryo, S., Ordoñez, L., Ariztegui, D., Henny, C., Crowe, S.A., Benning, L.G., Kallmeyer, J., Russell, J.M., Bijaksana, S., Vogel, H., the Towuti Drilling Project Science Team, 2019. Formation of diagenetic siderite in modern ferruginous sediments. *Geology* 47, 540–544. <https://doi.org/10.1130/G46100.1>.
- Waldmann, N., Stein, M., Ariztegui, D., Starinsky, A., 2009. Stratigraphy, depositional environments and level reconstruction of the last interglacial Lake Samra in the Dead Sea basin. *Quat. Res.* 72, 1–15. <https://doi.org/10.1016/j.yqres.2009.03.005>.
- Watkinson, I.M., Hall, R., 2019. Impact of communal irrigation on the 2018 Palu earthquake-triggered landslides. *Nat. Geosci.* 12, 940–945. <https://doi.org/10.1038/s41561-019-0448-x>.
- Watkinson, I.M., Hall, R., 2017. Fault systems of the eastern Indonesian triple junction: evaluation of Quaternary activity and implications for seismic hazards. *Geol. Soc. Lond. Spec. Publ.* 441, 71–120. <https://doi.org/10.1144/SP441.8>.
- Wicaksono, S.A., Russell, J.M., Holbourn, A., Kuhnt, W., 2017. Hydrological and vegetation shifts in the Wallacean region of central Indonesia since the last glacial maximum. *Quat. Sci. Rev.* 157, 152–163. <https://doi.org/10.1016/j.quascirev.2016.12.006>.
- Wierner, G., Moernaut, J., Stark, N., Kempf, P., De Batist, M., Pino, M., Urrutia, R., de Guevara, B.L., Strasser, M., Kopf, A., 2015. The role of sediment composition and behavior under dynamic loading conditions on slope failure initiation: a study of a subaqueous landslide in earthquake-prone South-Central Chile. *Int. J. Earth Sci.* 104, 1439–1457. <https://doi.org/10.1007/s00531-015-1144-8>.
- Wien, K., Holz, C., Kölling, M., Schulz, H.D., 2006. Age models for pelagites and turbidites from the cap timiris Canyon off Mauritania. *Mar. Petrol. Geol.* 23, 337–352. <https://doi.org/10.1016/j.marpetgeo.2005.10.005>.
- Wilhelm, B., Amann, B., Corella, J.P., Rapuc, W., Giguete-Coxev, C., Merz, B., Støren, E., 2022. Reconstructing paleoflood occurrence and magnitude from Lake sediments. *Quaternary* 5, 9. <https://doi.org/10.3390/quat5010009>.
- Wilhelm, B., Vogel, H., Anselmetti, F.S., 2017. A multi-centennial record of past floods and earthquakes in Valle d'Aosta, Mediterranean Italian Alps. *Nat. Hazards Earth Syst. Sci.* 17, 613–625. <https://doi.org/10.5194/nhess-17-613-2017>.
- Wilhelm, B., Vogel, H., Crouzet, C., Etienne, D., Anselmetti, F.S., 2016. Frequency and intensity of palaeofloods at the interface of Atlantic and Mediterranean climate domains. *Clim. Past* 12, 299–316. <https://doi.org/10.5194/cp-12-299-2016>.
- Wilhelm, Nomade, J., Crouzet, C., Litty, C., Sabatier, P., Belle, S., Rolland, Y., Revel, M., Courboux, F., Arnaud, F., Anselmetti, F.S., 2016. Quantified sensitivity of small lake sediments to record historic earthquakes: implications for paleoseismology: lake sensitivity to record earthquakes. *J. Geophys. Res. Earth Surf.* 121, 2–16. <https://doi.org/10.1002/2015JF003644>.
- Willemann, R.J., Storchak, D.A., 2001. Data collection at the international seismological centre. *Seismol. Res. Lett.* 72, 440–453. <https://doi.org/10.1785/gssrl.72.4.440>.
- Wils, K., Daryono, M.R., Praet, N., Santoso, A.B., Dianto, A., Schmidt, S., Vervoort, M., Huang, J.-S., Kusmanto, E., Suandhi, P., Natawidjaja, D.H., De Batist, M., 2021a. The sediments of Lake Singkarak and Lake Maninjau in West Sumatra reveal their earthquake, volcanic and rainfall history. *Sediment. Geol.* 416, 105863. <https://doi.org/10.1016/j.sedgeo.2021.105863>.
- Wils, K., Deprez, M., Kissel, C., Vervoort, M., Van Daele, M., Daryono, M.R., Cnudde, V., Natawidjaja, D.H., De Batist, M., 2021b. Earthquake doublet revealed

- by multiple pulses in lacustrine seismo-turbidites. *Geology* 49, 1301–1306. <https://doi.org/10.1130/G48940.1>.
- Wils, K., Van Daele, M., Kissel, C., Moernaut, J., Schmidt, S., Siani, G., Lastras, G., 2020. Seismo-turbidites in aysén fjord (southern Chile) reveal a complex pattern of rupture modes along the 1960 megathrust earthquake segment. *J. Geophys. Res. Solid Earth* 125, e2020JB019405. <https://doi.org/10.1029/2020JB019405>.
- Windler, G., Tierney, J.E., Zhu, J., Poulsen, C.J., 2020. Unraveling glacial hydroclimate in the indo-pacific warm pool: perspectives from water isotopes. *Paleoceanogr. Paleoclimatol.* 35, e2020PA003985. <https://doi.org/10.1029/2020PA003985>.
- Wu, D., Ren, Z., Liu, J., Chen, J., Guo, P., Yin, G., Ran, H., Li, C., Yang, X., 2021. Coseismic surface rupture during the 2018 Mw 7.5 Palu earthquake, Sulawesi island, Indonesia. *GSA Bull* 133, 1157–1166. <https://doi.org/10.1130/B35597.1>.